



Scaling carbon fluxes from eddy covariance sites to globe: Synthesis and evaluation of the FLUXCOM approach

Martin Jung¹, Christopher Schwalm², Mirco Migliavacca¹, Sophia Walther¹, Gustau Camps-Valls³,
Sujan Koirala¹, Peter Anthoni⁴, Simon Besnard^{1,5}, Paul Bodesheim^{1,6}, Nuno Carvalhais^{1,7}, Frédéric
5 Chevallier⁸, Fabian Gans¹, Daniel S. Goll⁹, Vanessa Haverd¹⁰, Philipp Koehler¹¹, Kazuhito Ichii^{12,13},
Atul K. Jain¹⁴, Junzhi Liu^{1,15}, Danica Lombardozzi¹⁶, Julia E.M.S. Nabel¹⁷, Jacob A. Nelson¹, Michael
O'Sullivan¹⁸, Martijn Pallandt¹⁹, Dario Papale^{20,21}, Wouter Peters²², Julia Pongratz^{23,17}, Christian
Rödenbeck¹⁹, Stephen Sitch¹⁸, Gianluca Tramontana^{20,3}, Anthony Walker²⁴, Ulrich Weber¹, Markus
Reichstein¹

10

¹Department of Biogeochemical Integration, Max Planck Institute for Biogeochemistry, Jena, 07745, Germany

²Woods Hole Research Center, Falmouth, MA, 02540-1644, USA

³Image Processing Laboratory (IPL), Universitat de València, Paterna, 46980, Spain

15 ⁴Institute of Meteorology and Climate Research – Atmospheric Environmental Research (IMK-IFU), Karlsruhe
Institute of Technology, Garmisch-Partenkirchen, 82467, Germany

⁵Laboratory of Geo-Information Science and Remote Sensing, Wageningen University and Research,
Wageningen, 6708 PB, Netherlands

⁶Department of Mathematics and Computer Science, Friedrich-Schiller Universität Jena, Jena, 07743, Germany

20 ⁷Departamento de Ciências e Engenharia do Ambiente (DCEA), Faculdade de Ciências e Tecnologia, FCT,
Universidade Nova de Lisboa, Caparica, 2829-516, Portugal

⁸Laboratoire des Sciences du Climat et de l'Environnement (LSCE/IPSL), Université Paris-Saclay, Gif-sur-
Yvette, F-91198, France

⁹Department of Geography, University of Augsburg, Augsburg, 86159, Germany

¹⁰Department Continental Biogeochemical Cycles, CSIRO Oceans and Atmosphere, Canberra, 2601, Australia

25 ¹¹Division of Geological and Planetary Sciences, California Institute of Technology, Pasadena, USA

¹²Center for Environmental Remote Sensing (CEReS), Chiba University, Chiba, 263-8522, Japan

¹³Center for Global Environmental Research, National Institute for Environmental Studies, Tsukuba, 305-8506,
Japan

¹⁴Department of Atmospheric Science, University of Illinois, Urbana, IL 61801, USA

30 ¹⁵School of Geography, Nanjing Normal University, Nanjing, 210023, China

¹⁶Climate and Global Dynamics Laboratory, National Center for Atmospheric Research, Boulder, CO 80307,
USA

¹⁷Department Land in the Earth System (LES), Max Planck Institute for Meteorology, Hamburg, 20146,
Germany

35 ¹⁸College of Life and Environmental Sciences, University of Exeter, Exeter, EX4 4QE, UK

¹⁹Department of Biogeochemical Systems, Max Planck Institute for Biogeochemistry, Jena, 07745, Germany

²⁰Department of Innovation in Biology, Agri-food and Forest systems (DIBAF), University of Tuscia, Viterbo,
01100, Italy

40 ²¹Impacts on Agriculture, Forests and Ecosystem Services (IAFES), EuroMediterranean Center on Climate
Change (CMCC), Lecce, 01100, Italy



²²Department of Meteorology and Air Quality, Wageningen University and Research, Wageningen, 6700 AA, Netherlands

²³Department of Geography, Ludwig-Maximilians-Universität München, München, 80333, Germany

²⁴Climate Change Science Institute, Oak Ridge National Laboratory, Oak Ridge, USA

45 *Correspondence to:* Martin Jung (mjung@bgc-jena.mpg.de)

Abstract. FLUXNET assembles globally-distributed eddy covariance-based estimates of carbon fluxes between the biosphere and the atmosphere. Since eddy covariance flux towers have a relatively small footprint and are distributed unevenly across the world, upscaling the observations is necessary in order to obtain global-scale estimates of biosphere-atmosphere exchange from the flux tower network. Based on cross-consistency checks with atmospheric inversions, sun-induced fluorescence (SIF) and dynamic global vegetation models (DGVM), we provide here a systematic assessment of the latest upscaling efforts for gross primary production (GPP) and net ecosystem exchange (NEE) of the FLUXCOM initiative, where different machine learning methods, forcing datasets, and sets of predictor variables were employed.

Spatial patterns of mean GPP are consistent among FLUXCOM and DGVM ensembles ($R^2 > 0.94$ at 1° spatial resolution) while the majority of DGVMs are outside the FLUXCOM range for 70% of the land surface. Global mean GPP magnitudes for 2008–2010 from FLUXCOM members vary within 106 and 130 PgC yr⁻¹ with the largest uncertainty in the tropics. Seasonal variations of independent SIF estimates agree better with FLUXCOM GPP (mean global pixel-wise $R^2 \sim 0.75$) than with GPP from DGVMs (mean global pixel wise $R^2 \sim 0.6$). Seasonal variations of FLUXCOM NEE show good consistency with atmospheric inversion-based net land carbon fluxes, particularly for temperate and boreal regions ($R^2 > 0.92$). Interannual variability of global NEE in FLUXCOM is underestimated compared to inversions and DGVMs. The FLUXCOM version which uses also meteorological inputs shows a strong co-variation of interannual patterns with inversions ($R^2 = 0.88$ for 2001–2010). Mean regional NEE from FLUXCOM shows larger uptake than inversion and DGVM-based estimates, particularly in the tropics with discrepancies of up to several hundred gC m² yr⁻¹. These discrepancies can only partly be reconciled by carbon loss pathways that are implicit in inversions but not captured by the flux tower measurements such as carbon emissions from fires and water bodies. We hypothesize that a combination of systematic biases in the underlying eddy covariance data, in particular in tall tropical forests, and a lack of site-history effects on NEE in FLUXCOM are likely responsible for the too strong tropical carbon sink estimated by FLUXCOM. Furthermore, as FLUXCOM does not account for CO₂ fertilization effects carbon flux trends are not realistic. Overall, current FLUXCOM estimates of mean annual and seasonal cycles of GPP as well as seasonal NEE variations provide useful constraints of global carbon cycling, while interannual variability patterns from FLUXCOM are valuable but require cautious interpretation. Exploring the diversity of Earth Observation data and of machine learning concepts along with improved quality and quantity of flux tower measurements will facilitate further improvements of the FLUXCOM approach overall.



1 Introduction

Upscaling local eddy covariance (EC) measurements from tower footprint to global wall-to-wall maps uses globally-available predictor variables such as satellite remote sensing and meteorological data. This forcing data is first used to establish empirical models for fluxes of interest at site level, and then to estimate gridded fluxes by applying these models across all vegetated grid cells. Previous FLUXNET upscaling efforts using machine learning techniques (Beer et al., 2010; Jung et al., 2009; Jung et al., 2011) yielded global products that present a data-driven ‘bottom-up’ perspective on carbon fluxes between the biosphere and the atmosphere. These ‘bottom-up’ products are complementary to process-based model simulations and ‘top-down’ atmospheric inversions. However, estimates of carbon fluxes are subject to uncertainty from choice of machine learning algorithm and predictor variables, forcing data, FLUXNET measurements and incomplete representation of the different ecosystems therein. The FLUXCOM initiative (www.fluxcom.org) aims to improve our understanding of the multiple sources and facets of uncertainties in empirical upscaling and, ultimately, to provide an ensemble of machine learning-based global flux products to the scientific community. Within FLUXCOM an intercomparison was conducted for two complementary experimental setups of input drivers and resulting global gridded products. These setups systematically vary machine learning and flux partitioning methods as well as forcing datasets to separate measured net ecosystem exchange (NEE) into gross primary productivity (GPP) and Terrestrial Ecosystem Respiration (TER) (Jung et al., 2019; Tramontana et al., 2016).

Evaluating the strengths and weaknesses of the FLUXCOM products and the approaches used therein is crucial to inform potential scientific uses, and to guide future methodological developments. An evaluation based on site-level cross-validation analysis (Tramontana et al., 2016) showed a general high consistency among machine learning algorithms, experimental setups and flux partitioning methods applied in FLUXCOM. However, the conclusions from site-level cross-validation may be limited by potential systematic measurement errors that are inherent in the underlying EC measurements (e.g. Aubinet et al., 2012), or the spatially biased distribution of FLUXNET sites (Papale et al., 2015). Therefore, cross-consistency checks of the FLUXCOM products with independent estimates are important to consider. But such checks are complex due to limitations of the independent approaches or the lack of comparability of similar but not identical variables. In this study, we contextualize FLUXCOM products in relation to independent state-of-the-art estimates of carbon cycling. The comparison strategy prioritises robust features of the independent datasets, and discusses residual uncertainties.

The objectives of this paper are a) to present a synthesis and evaluation of FLUXCOM ensembles for GPP and NEE against patterns of remotely sensed sun induced fluorescence (SIF) and atmospheric inversion results respectively, b) to discuss limitations of FLUXCOM and synthesize lessons learned, and c) to outline potential future paths of FLUXCOM development. Due to limitations of the SIF product with respect to interannual variability (Zhang et al., 2018), the evaluation of GPP against SIF is restricted to seasonal variations of photosynthesis. To reduce the impact of atmospheric transport-



105 related uncertainties of inversion products, mean annual and seasonal variations of NEE are compared at the regional scales,
and interannual variability is assessed at global scale. In addition, we contextualize our comparisons with FLUXCOM by
providing comparisons with the previous Model Tree Ensemble (MTE) results of Jung et al., 2011 (Ju11) as well as an
ensemble of process-based Global Dynamic Vegetation Model (DGVM) simulations from the TRENDY DGVM Projects
(Le Quéré et al., 2018; Sitch et al., 2015). Even though FLUXCOM also produced global products of TER, these are not
110 shown here due to a lack of an independent observational benchmark.

2 Data and methods

2.1 FLUXCOM

We used the cross-validated and trained machine learning techniques for the FLUXCOM carbon fluxes of Tramontana et al.
(2016) and generated large ensembles ($n = 120$) of global gridded flux products for two different setups: remote sensing (RS)
115 and remote sensing plus meteorological/climate forcing (RS+METEO) setups (Figure 1). In the RS setup, fluxes are
estimated exclusively from Moderate Resolution Imaging Spectroradiometer (MODIS) satellite data. In RS+METEO fluxes
are estimated from mean seasonal cycles of the satellite data and daily meteorological information (see Table S1). For the
rationale of these setups, we refer the interested reader to Tramontana et al., 2016 and Jung et al., 2019. For the RS setup,
nine machine learning methods were used to generate gridded products at an 8-daily temporal and 0.0833° spatial resolution
120 for the 2001-2015 period. For the RS+METEO setup, three machine learning methods with five global climate forcing data
sets (Table 1) yielded products with daily temporal and 0.5° spatial resolution and time periods depending on the
meteorological data. The meteorological data included WATCH Forcing Data-ERA Interim (WFDEI; Weedon et al., 2014),
Global Soil Wetness Project 3 forcing data (GSWP3, Kim, 2017), CRU-JRA version 1.1 (Harris, 2019), ERA5 ((C3S),
2017), and a combination of observation-based radiation from CERES (Doelling et al., 2013) and precipitation from GPCP
125 (Huffman et al., 2001) (CERES-GPCP) resampled to 0.5° . The wide range of data sources from reanalysis to station
measurements to satellite observation is intentional and is meant to bracket potential uncertainties in meteorological forcing.

For GPP and TER, we additionally considered uncertainty from flux partitioning methods by propagating two different
variants, one based on night-time NEE data (Reichstein et al., 2005) and one on daytime data (Lasslop et al., 2010). Within
130 the RS and RS+METEO setups, we followed a full factorial design of machine learning methods (9 for RS, 3 for
RS+METEO) times flux partitioning variants (2 for GPP and TER), and climate forcing input products (5, only for
RS+METEO). Details of machine learning training setup, and validation are available in Tramontana et al., 2016. The
methodology of generating the global products is documented in detail in the overview paper on global energy fluxes from
FLUXCOM (Jung et al., 2019). The details of machine learning training setup, and validation are available in Tramontana et
135 al., 2016.



To allow for a better reuse of the large archive, we generated ensemble products of monthly values where individual ensemble members were first aggregated to monthly means (Figure 1). The ensemble products encompass estimates of different machine learning estimates, flux partitioning variants for GPP and TER, and different climate input data for
140 RS+METEO. For the RS+METEO setup, this was also done separately for each climate forcing data to allow modellers to compare their simulations with the FLUXCOM ensemble product driven by the same forcing. The ensemble products (hereafter referred as FLUXCOM-RS and FLUXCOM-RS+METEO) were generated as the median over ensemble members for each grid cell and month. The FLUXCOM-RS products are based on 9 ensemble members for NEE and on 18 for GPP and TER. The FLUXCOM-RS+METEO is based on 15 ensemble members for NEE and on 30 for GPP and TER.

145 2.2 Process-model simulations (TRENDY)

Dynamic Global Vegetation Models (DGVMs) represent an independent, process-based and bottom-up approach to represent the terrestrial carbon cycle and its evolution with changing environmental conditions. Here we use data from an ensemble of 16 DGVMs that were forced with the same climate (CRU-JRA v1.1), global atmospheric CO₂ concentration, and land-use and land cover change data (S3 simulation) over the period 1700 – 2017, following a common protocol
150 (TRENDY-v7) (Le Quéré et al., 2018; Sitch et al., 2015). This ensemble provides fluxes at a monthly temporal resolution harmonized to a common 1° spatial resolution with simulations from: CABLE-POP, CLASS-CTEM, CLM5.0, DLEM, ISAM, JSBACH, JULES, LPJ-GUESS, LPJ, OCN, ORCHIDEE-CNP, ORCHIDEE-Trunk, SDGVM, SURFEX and VISIT. TER was calculated as the sum of heterotrophic and autotrophic respiration; NEE as heterotrophic respiration minus net primary productivity. NBP from models incorporates additional fluxes as well: fire emissions (10 DGVMs), land use change
155 (all DGVMs), harvest (14 DGVMs), grazing (6 DGVMs), and any other carbon flux in/out of the ecosystem (e.g. erosion, 1 DGVM, VISIT). LPJ-GUESS was excluded from comparisons of NEE or NBP since monthly output on heterotrophic respiration was not available.

2.3 Independent observation-based products

For the comparison with GPP, we used gridded monthly SIF GOME-2 (Köhler et al., 2015) retrievals from the far-red
160 spectral range, and for the evaluation of NEE atmospheric inversion-based estimates from Jena CarboScope (Rödenbeck et al., 2018), CAMSv17r1 (Chevallier et al., 2005; Chevallier et al., 2019), and CarbonTracker-EU (CTE2018, Peters et al., 2010; van der Laan-Luijkx et al., 2017). We further include comparisons to the previous GPP and NEE upscaling products of Jung et al., 2011 (hereafter referred as Ju11).



2.4 Comparison approach

165 2.4.1 General considerations

All products were harmonized to a common 1° spatial resolution with monthly temporal resolution as a basis of all comparisons shown here. Cross-consistency checks for mean annual and mean seasonal variations of GPP and NEE are based on the three year period 2008-2010. The time period is constrained by the availability of GOME-2 data starting in 2008 and the corresponding end year of the RS+METEO ensemble with the GSWP3 forcing ending in 2010. The NEE interannual variability was initially assessed for 2001-2010 which is the common period of the RS and RS+METEO ensembles while comparisons for longer-time periods were also facilitated by using meteorological forcing specific RS+METEO products that cover longer time periods (Table 1).

FLUXCOM-RS and FLUXCOM-RS+METEO products are evaluated mostly separately. We report estimates for the respective ensemble product (see section 2.1): the spread over individual ensemble members for uncertainty and the mean of the ensemble members; the latter can be different from the ensemble product estimate (see Sect.2.1). Occasionally, we use the range of estimates from the union of RS and RS+METEO ensemble members to show the full FLUXCOM uncertainty range across the two setups (labelled as “FLUXCOM” only). For the comparison of regional or global flux values, we used flux densities rather than integrated fluxes due to inconsistencies in land-sea masks in different products. A common mask of valid data from the intersection of FLUXCOM, TRENDY, and Ju11 was applied to all data streams, and a land area-weighted regional or global mean calculated. Globally integrated GPP was calculated by scaling the global mean GPP density flux with the global non-barren land area (122.4 Mio km²) derived from the MODIS land cover product (Friedl et al., 2010). All reported R² values are squared Pearson’s correlation coefficients but negative correlation signs are maintained through by multiplying R² values by -1. We aimed at structuring the cross-consistency checks with SIF and inversion data to minimize confounding factors and uncertainties of the independent data that may have affected the conclusions otherwise.

185 2.4.2 Rationale of GPP-SIF comparison

As the GPP-SIF relationship is approximately linear over seasonal time scales (Zhang et al., 2016), the comparison was based on monthly values. To minimize confounding effects of canopy structure (e.g. Migliavacca et al., 2017), the comparisons were done over time when canopy structure changes relative to GPP changes are expected to be much weaker than spatial changes. The unstable orbit of the MetOp-A satellite that carries one of the GOME-2 instruments and sensor degradation effects do not permit conclusive comparisons with respect to interannual variability (Zhang et al., 2018). Therefore, we restricted the analysis to mean seasonal cycles and show 1° maps of the R² between mean monthly GPP and SIF.



195 There are remaining caveats and uncertainties associated with the GPP-SIF relationship (see e.g. Porcar-Castell et al., 2014
for an overview). Nevertheless, various studies have shown that SIF is currently the best proxy for photosynthesis that can be
remotely-sensed directly, in particular at seasonal time scale and over regions with strong seasonal cycles. This is supported
by strong empirical relationships between GPP and SIF across different satellites and retrieval methods as well as from EC
data, crop inventories, and data-driven GPP methods (Frankenberg et al., 2011; Guanter et al., 2014; Joiner et al., 2018; Sun
200 et al., 2017; Walther et al., 2016). This gives us confidence in using SIF as an independent data stream for photosynthesis to
evaluate FLUXCOM products.

2.4.3 Rationale of comparing net carbon fluxes with atmospheric inversions

We compared atmospheric inversion-based net carbon release with FLUXCOM mean NEE at the seasonal scale over the
established 11 TRANSCOM regions (see Fig.S1 for a map) as atmospheric inversions are better constrained over large
205 spatial scales (Peylin et al., 2013). The comparison of interannual variability was conducted at global scale due to its smaller
signal and larger transport uncertainties compared to the seasonal cycle. Due to various inversion uncertainties related to
choices of atmospheric transport model, atmospheric station CO₂ data, fossil fuel information, prior constraints, driving wind
fields, and inversion strategy, we used three different products: Jena CarboScope (s99oc_v4.3, Rödenbeck et al., 2018),
CAMsv17r1 (Chevallier et al., 2005; Chevallier et al., 2019), and CarbonTracker-EU (CTE2018, Peters et al., 2010; van der
210 Laan-Luijkx et al., 2017). To evaluate global NEE interannual variability patterns for periods since the late 1950s until
present, we further use two long-term atmospheric inversions (CarboScope s57Xoc_v4.3, sEXTocNEET_v4.3, Rödenbeck et
al., 2018) and annual CO₂ growth rate from the Global Carbon Budget (Le Quéré et al., 2018).

It is important to note that FLUXCOM NEE is semantically different from inversion-based net carbon exchange between
215 land and atmosphere. The former is solely the difference between gross fluxes (i.e., $NEE = TER - GPP$) while the latter
integrates all vertical movement of CO₂ including, for example, fire emissions, evasion from inland waters, respired harvests,
or volatile organic compounds (Kirschbaum et al., 2019; Zscheischler et al., 2017). Simulations from TRENDY models
report both, NEE and net biome productivity (NBP) which is conceptually close but not identical to what atmospheric
inversions provide. To assess whether conclusions are affected by the different NEE vs NBP definitions we a) provide NEE
220 and NBP estimates from TRENDY models, b) we include comparisons where inversions were corrected for fire emissions
(from CarbonTracker-EU) to yield estimates closer to NEE, and c) discuss whether discrepancies with FLUXCOM can
originate from the omission of secondary carbon loss pathways given in the literature.



3 Results and discussion

3.1 Gross primary productivity

225 3.1.1 Mean annual gross primary productivity

Overall, our results suggest a high degree of cross-product (and, for FLUXCOM, also within-product) consistency of global mean GPP patterns (Figure 2). In fact, global patterns of mean GPP are consistent across both FLUXCOM ensembles ($R^2=0.97$) as well as for Ju11 and TRENDY ensemble mean ($R^2>0.94$), despite sizeable regional differences. The slope of the pair-wise 1:1 regressions among the different mean GPP data sets varies within ~10%. FLUXCOM-RS shows about 10-
230 20% lower GPP than FLUXCOM-RS+METEO in the highly productive tropics and some subtropical regions. Both FLUXCOM setups estimate larger GPP than Ju11 and TRENDY in some semi-arid regions and about 5-15% lower GPP in some extratropical areas. Despite a sizeable total range of mean GPP from all 48 FLUXCOM members, the majority of TRENDY models (at least 9 out of 16) fall outside the FLUXCOM range for about 70% of the land surface (Figure 3).

235 The mean global GPP of FLUXCOM-RS (111 PgC yr^{-1}) is about 10% lower than RS+METEO (120 PgC yr^{-1} , Figure 4), which is largely driven by differences in the tropics (Figure 2). The cross-validation analysis indicated an underestimation of FLUXCOM-RS GPP in the tropics (Tramontana et al., 2016), which was confirmed by a grid cell-to-site data comparison for the FLUXNET 2015 data (which were not used for machine learning training here) (Joiner et al., 2018). The reasons for the on-average lower GPP of RS compared to RS+METEO require further investigation. It is unlikely that the smaller RS GPP
240 values are because this setup is exclusively based on remote sensing, as global latent heat from RS was larger than Ju11 (Jung et al., 2019). It seems to be rather related to the specifically different predictor sets between RS and RS+METEO. This indicates that future FLUXCOM efforts should expand the ensemble with respect to predictor set diversity to better account for this source of uncertainty in upscaling. Focussing on FLUXCOM-RS+METEO, its ensemble spread ($108\text{-}130 \text{ PgC yr}^{-1}$) is much smaller than the TRENDY-based global GPPs ($83\text{-}172 \text{ PgC yr}^{-1}$), and is primarily due to differences among machine
245 learning methods rather than meteorological forcing data (Fig.S2).

Our results imply that the present FLUXNET upscaling approach does not agree with larger GPP values of $150\text{-}175 \text{ PgC yr}^{-1}$ derived from an isotope-based study (Welp et al., 2011). It is possible that the FLUXNET upscaling approach underestimates GPP of highly managed and fertilized crops (Guanter et al., 2014) but their effects on global GPP biases seem small (Joiner
250 et al., 2018). At FLUXNET sites night-time CO_2 advection and storage could cause underestimation of night-time CO_2 fluxes (Aubinet et al., 2012; McHugh et al., 2017; van Gorsel et al., 2009) and thus underestimate GPP using the night-time NEE flux partitioning method. On the contrary, it has been suggested that FLUXNET GPP estimated from the night-time partitioning method (Reichstein et al., 2005) is overestimated as it ignores the effects of light inhibition of leaf respiration (Keenan et al., 2019; Wehr et al., 2016) by on average 7% across FLUXNET sites (Keenan et al., 2019). But it should be
255 noted that this value may not be globally representative due to sizeable variations between ecosystems and with leaf area.



Further, we only find a small difference of mean global GPP of <2 PgC for day-time (Lasslop et al., 2010) and night-time (Reichstein et al., 2005) NEE partitioning. This suggests that neither CO_2 advection nor the light inhibition of leaf respiration appear to generate sizeable biases of global GPP in FLUXCOM—a tendency likely encouraged by the relatively strict quality control on the EC fluxes data (Tramontana et al., 2016). Furthermore, a comparison of EC-based GPP with biometric
260 GPP estimates across 18 globally distributed sites showed good agreement and no significant bias (Campioli et al., 2016). A recent study using Carbonyl Sulfide (COS)-based partitioning for four contrasting European sites also showed good agreement with standard EC-based GPP where systematic differences for mean GPP were $< 5\%$ (Spielmann et al., 2019). Therefore, we currently have no strong indication that systematic biases of FLUXNET GPP propagate to global FLUXCOM GPP. Nevertheless, we need to acknowledge that global GPP is largely driven by the productivity in the tropics where flux
265 towers are scarce and may be particularly uncertain due to challenging logistic and micrometeorological conditions (Fu et al., 2018).

Various remote sensing-based light use efficiency approaches, calibrated with flux tower data, yielded global GPP estimates of 109 (Zhao et al., 2005), 111 ± 21 (Yuan et al., 2010), 108-119 (Yu et al., 2018), 122 ± 25 (Jiang and Ryu, 2016), 132 ± 22
270 (Chen et al., 2012), and 140 PgC yr^{-1} (Joiner et al., 2018). A simple calibration of only near-infrared reflectance (NIRv) to EC data suggested a global GPP of 131-163 PgC yr^{-1} (Badgley et al., 2019). Studies that assimilated atmospheric CO_2 concentration data into process model simulations yielded slightly higher values of 148 (Anav et al., 2015) and $146 \pm 19 \text{ PgC yr}^{-1}$ (Koffi et al., 2012) with the latter study unable to distinguish their best estimate from a global GPP of 117 PgC yr^{-1} because the atmospheric CO_2 alone cannot constrain magnitudes of gross fluxes well. Assimilating SIF into process-models
275 yielded 137 ± 6 (Norton et al., 2019) and $166 \pm 10 \text{ PgC yr}^{-1}$ (MacBean et al., 2018), while constraining GPP magnitudes with SIF should be very uncertain. More recent isotope studies derived global GPP as $120 \pm 30 \text{ PgC yr}^{-1}$ (Liang et al., 2017), and global NPP of $\sim 60 \text{ PgC yr}^{-1}$ (Hellevang and Aagaard, 2015) which implies global GPP of 109-150 PgC yr^{-1} considering a range of NPP:GPP ratios of 0.4-0.55. In conclusion, global FLUXCOM GPP estimates are within the currently most plausible 110-150 PgC yr^{-1} range.

280 3.1.2 Seasonal cycles of gross primary productivity

Cross-consistency analysis of mean monthly GPP seasonal cycles from FLUXCOM with SIF from GOME-2 (Köhler et al., 2015) shows widespread and strong agreement for both FLUXCOM setups (Figure 5), except for the inner tropics where seasonality is weak and SIF retrievals might be affected by the South Atlantic Magnetic Anomaly (Köhler et al., 2015). FLUXCOM-RS tends to show better agreement with SIF than FLUXCOM-RS+METEO in agricultural regions of Southeast
285 Asia, maybe because only the mean seasonal cycles of remotely sensed land surface properties were used in the latter. Conversely, FLUXCOM RS+METEO shows on average better consistency with SIF in some semi-arid regions, e.g., Australia. However, maps of the maximum R^2 with SIF for RS and RS+METEO respectively have similar patterns with good agreement of both products in Australia, and even in the tropics (Fig.S3). This suggests that the inclusion of some



290 machine learning methods somewhat negatively impacts the ensemble, especially for RS which shows larger spread (see Fig.S4 for mean R^2 of the RS ensemble members). With SIF, both FLUXCOM setups show similar consistency as Ju11. The consistency of FLUXCOM with SIF is much better than with TRENDY models, in particular in tropical and subtropical regions. This implies that, despite sporadic spatial coverage of FLUXNET sites and previously identified incomplete capturing of water stress (Bodesheim et al., 2018; Tramontana et al., 2016), FLUXCOM still has a large potential to inform and constrain process-based model simulations of seasonal variations of photosynthesis in moisture-limited regions.

295 3.2 Net ecosystem exchange

3.2.1 Mean annual net ecosystem exchange

300 In most TRANSCOM regions, FLUXCOM shows a stronger mean annual net carbon uptake than indicated by atmospheric inversions with a particularly large systematic difference in the tropics (Figure 6). This pattern of a large tropical carbon sink in FLUXCOM is qualitatively consistent among the different FLUXCOM setups and ensemble members, as well as with previous estimates from Ju11. To date, this is a systematic feature of the current data-driven approach of upscaling EC measurements with machine learning.

305 Multiple independent approaches indeed imply a sizeable carbon sink in intact tropical forests (Arneeth et al., 2017; Gaubert et al., 2019; Pan et al., 2011), which appears to be largely or entirely offset by carbon loss pathways in the tropical region such as fire, land-use change emissions, and evasion from inland waters. These CO_2 sources are not sampled by EC measurements from FLUXNET, and are, therefore, not represented in FLUXCOM. These missing fluxes can resolve only up to roughly half of the gap (Zscheischler et al., 2017). The comparatively small differences between net carbon release estimates by inversions and those where fire emissions were corrected for, as well as the small differences between NEE and $-\text{NBP}$ from TRENDY further suggest that these secondary carbon loss fluxes are likely not dominating the large discrepancy 310 between FLUXCOM and inversion-based mean net carbon exchange. Nevertheless, substantial uncertainty remains in the magnitude of these secondary carbon fluxes and their accounting in TRENDY models and inversions is also incomplete (Kirschbaum et al., 2019; Zscheischler et al., 2017).

315 Issues with the current FLUXCOM approach certainly contribute, likely dominate, the discrepancy between atmospheric top-down and FLUXCOM mean NEE. Potential factors that could contribute to this are 1) a FLUXNET sampling bias (see also Sect. 4.1.2) towards ecosystems with a large carbon sink, particularly in the tropics (Saleska et al., 2003); combined with 2) missing predictor variables related to disturbance and site-history (Amiro et al., 2010; Besnard et al., 2018, see also Sect. 4.2.1), or 3) biases of eddy covariance NEE measurements, e.g. due to night-time advection of CO_2 (Hayek et al., 2018; van Gorsel et al., 2008), especially under tall tropical forest canopies (Hutyra et al., 2008, Fu et al., 2018). Fu et al. (2018) 320 studied 63 site-years of EC data from 13 tropical forest sites and report a mean between-site NEE of $-567 \text{ gC m}^{-2} \text{ yr}^{-1}$



showing that the large tropical sink in FLUXCOM is inherited from FLUXNET data. The authors pointed out that for about half of the sites where measurements of CO₂ concentration along the vertical profile were available and the storage was considered in the NEE processing, the carbon sink was less than half (-340 gC m⁻² yr⁻¹) compared to those without storage correction (-832 gC m⁻² yr⁻¹). However, the small sample size together with the large between-site standard deviation of mean NEE (459 gC m⁻² yr⁻¹) not only makes robust conclusions difficult, but also indicates potentially large diversity between tropical ecosystems. Clearly, more tropical EC sites are needed along with a better accounting of systematic errors in EC-based NEE measurements to resolve this issue.

3.2.2 Seasonal cycles of net ecosystem exchange

We find a good consistency between FLUXCOM and inversions with respect to amplitude and shape of the seasonal cycles of NEE in many TRANSCOM regions, especially over the North American Boreal, North American Temperate, and Europe regions with R² values > 0.92 (Figure 7). As with mean annual NEE, the seasonal cycle mismatch relative to inversions may be linked to carbon loss fluxes not accounted for in FLUXCOM, such as fire emissions that are seasonally relevant in tropical and subtropical regions. However, adjusting inversion-based NBP towards NEE by correcting for fire emissions does not improve the correspondence with FLUXCOM in tropical and subtropical regions (Fig.S5). In tropical regions, the weak seasonality paired with comparatively large spread among inversions does not allow for robust conclusions. Overall, the seasonal variations of FLUXCOM NEE show potential to constrain the large uncertainty in TRENDY models, and potentially even atmospheric inversions at the regional scale, especially considering that their uncertainty range across only three products is still significant.

3.2.3 Interannual variability of net ecosystem exchange

Spatial patterns of the magnitude of the interannual variability (IAV) of land carbon sink for the period 2001-2010 share some common features among atmospheric inversions, FLUXCOM-RS, FLUXCOM-RS+METEO and TRENDY. For example, all products identify the hotspots in southeast Asia, southern North America, and also in the Siberian tundra (Figure 8). Overall, there are still differences in the spatial patterns of IAV magnitude among and within different data-streams.

All EC data-driven methods, in particular FLUXCOM-RS+METEO, underestimate magnitude of IAV compared to inversions (Figure 8). The reasons for the underestimation of IAV magnitude by FLUXCOM are not fully clear. Within FLUXCOM, the smaller IAV magnitude of RS+METEO NEE compared to that of RS is linked to the use of only mean seasonal cycles of RS-based land surface properties in RS+METEO setup. The IAV of carbon loss fluxes that are not captured by FLUXCOM, such as through fire, are currently thought to be comparatively small at the global scale and appear minor here (see Fig.S6). Machine learning methods already underestimate the IAV at the site level (Marcolla et al., 2017; Tramontana et al., 2016). The low bias in FLUXCOM IAV is a direct consequence of the comparatively small explained



variance for NEE anomalies. Thus, improving the predictability of NEE IAV at site level has potential to also correct the magnitude of globally integrated IAV variance.

355

Despite the tendency of FLUXCOM products to underestimate IAV magnitude, FLUXCOM-RS+METEO reproduces year-to-year variations of globally integrated annual land carbon exchange anomalies derived from atmospheric inversions for 2001-2010 ($R^2=0.88$). It shows better consistency than TRENDY with one of the long-term inversions (Fig.S7). Further examination of this ensemble reveals that the choice of machine learning method, rather than meteorological forcing data, has a larger influence on IAV of global NEE (Fig.S8). Here, the Random Forests method performed comparatively poor. Interestingly, training Random Forests with an almost identical predictor set but at half-hourly temporal scale rather than at daily scale (Bodesheim et al., 2018) substantially improved the R^2 (from 0.31 to 0.60, Fig.S8). This indicates that machine learning methods can benefit from higher temporal variability provided by millions of high-frequency NEE measurements, especially for signals such as IAV that are small and difficult to extract. In addition, underlying functional relationships can be better extracted from high-frequency data as the predictor space is better covered, allowing for improved discrimination of drivers that have stronger covariation on longer time-scales.

360
365

To better understand the qualitatively different global NEE IAV patterns between RS and RS+METEO setups, we infer which NEE IAV signals are consistent or lacking among FLUXCOM setups and TRENDY models by assessing correlation patterns (Figure 9). We find the strongest consistencies of NEE IAV between FLUXCOM-RS and FLUXCOM-RS+METEO in many semi-arid regions, and almost no consistency otherwise. This suggests that the main discrepancies of globally integrated NEE IAV between FLUXCOM-RS and FLUXCOM-RS+METEO are likely not due to differences in their capabilities of reflecting water stress effects. It has been shown that despite the local dominance, water-related NEE anomalies largely cancel spatially in RS+METEO and TRENDY resulting in the dominance of temperature-related NEE anomalies in globally integrated land sink IAV (Jung et al., 2017, but see Humphrey et al., 2018 for a different perspective). Studies on effects of water availability on spatial GPP anomalies using the RS data yielded highly plausible patterns that were consistent with independent data (Flach et al., 2018; Orth et al., in review; Walther et al., 2019). Also the comparison of FLUXCOM-RS GPP monthly anomalies with the independent FLUXNET2015 data set showed unexpected large consistency when anomalies were scaled by the site-specific observational range (Joiner et al., 2018). When delineating the regions with larger agreement between RS+METEO and TRENDY than that between RS and TRENDY, we can infer that FLUXCOM-RS seems to miss important NEE anomaly features in the tropics. This is likely due to (1) a combination of sparse satellite data availability, cloud contamination, and geometrical illumination effects in the tropics or (2) that the processes governing NEE IAV in the tropics cannot be captured by satellite-based predictors alone in RS (even under ideal observational conditions) but require additional meteorological variables such as temperature that is included in the RS+METEO setup. Some support for the latter point comes from Byrne et al., 2019 who found strong correlations of

370
375
380
385



anomalies from GOSAT inversions with NEE from RS+METEO and soil temperatures in the tropics but not with SIF and a drought indicator, suggesting that temperature impacts respiration more than photosynthesis in the tropics.

Overall there are large discrepancies among FLUXCOM and TRENDY as well as amongst TRENDY models with respect to local NEE IAV. This reflects our limited understanding and capabilities to model year-to-year variations of local ecosystem carbon exchange. Both data-driven and process-based approaches also showed poor performance with respect to NEE IAV in FLUXNET sites (Tramontana et al., 2016, Morales et al., 2005). However, both approaches yield good correspondence of globally integrated NEE with atmospherically-derived interannual land sink variations. This correspondence is due to two reasons: first, the spatial compensation of locally important processes that are not well captured by the models; and second, models capture better the temperature-related signals that gain relevance at larger spatial scales (Jung et al., 2017). Whether the large uncertainty of modelling NEE IAV at ecosystem level is due to misspecified parameterizations, missing predictors, inaccurate forcing data and/or absent processes remains a research priority. Our understanding and ability to model NEE IAV bottom-up would greatly benefit from atmospheric inversions that could localize NEE robustly. Exploiting the massive space-based column CO₂ data in the future will hopefully facilitate the improvements on this aspect. Despite large uncertainties and apparent knowledge gaps in NEE IAV from both an observational and modelling perspective, there are promising indications of improved capability to track IAV patterns with FLUXCOM such as the good correspondence of RS+METEO with inversions at global scale, and independent verifications of GPP IAV of RS at least outside the wet tropics (Flach et al., 2018; Joiner et al., 2018; Orth et al., in review; Walther et al., 2019).

4 Methodological limitations and potential ways forward

Machine learning methods can learn arbitrarily complex functions and provide a nearly perfect model of a phenomenon if they are fed with the right data and trained thoroughly. Thus the quality, quantity, and completeness of the input data determine the quality of the output. In the following, we discuss the relevance of limitations associated with data from the FLUXNET network, and of the limited capabilities of representing all relevant factors by observable predictor variables. We also outline potential strategies for improvements, both overall and with respect to machine learning approaches specifically. The continued and rapid development of machine learning notwithstanding, we believe that the FLUXCOM approach is at present more limited by available “information” rather than by available machine learning methods.

4.1 FLUXNET observations

4.1.1 Potential observation errors

The comparatively large random errors of high-frequency EC measurements diminish quickly when aggregated to daily or 8-daily averages used here. Furthermore, training on half-hourly EC data (Bodesheim et al., 2018) helps machine learning methods extract patterns from noisy data. In general, poor signal-to-noise ratios can be counteracted by larger sample size.



More problematic than random errors are potential systematic errors of EC measurements since those would propagate to the derived global carbon flux products. Even though there have been large efforts by the community to characterize and to correct for systematic errors, such as those due to low turbulence and CO₂ advection (e.g. Aubinet et al., 2005; Aubinet et al., 2012; Papale et al., 2006), uncertainties remain on the relevance and magnitude of those errors in the processed FLUXNET data. Differences due to instrumentation and maintenance pose another potential source of uncertainty. Additionally, the energy balance closure gap at FLUXNET sites is still not resolved (Stoy et al., 2013), while it remains unclear to what extent this is relevant for CO₂ fluxes (Leuning et al., 2012). Systematic errors in GPP and TER derived from the flux partitioning method of NEE based on night-time data (Reichstein et al., 2005) may arise due to the neglected effect of inhibited photorespiration during daytime (Keenan et al., 2019; Wehr et al., 2016). Nevertheless, all these issues together seem to be relatively small compared to the predominant patterns of variability in EC data, e.g., seasonal variations, that are very consistent across FLUXCOM and independent observation-based data streams shown here. The relatively strict quality controls on the flux training data (Tramontana et al., 2016) may have been instrumental here. The trade-off between data quality and training data volume was not explicitly studied in FLUXCOM, and related experimental setups would be desirable to gauge the robustness of the global products shown here. Even small systematic errors in EC data could degrade important signals such as interannual variability, trends, annual sums of NEE, or subtle differences between sites related to functional properties (e.g., radiation use efficiency). Systematic errors that would be prevalent across the network would result in systematic biases of derived global fluxes. For global GPP and energy fluxes (Jung et al., 2019), the values obtained from FLUXCOM are generally consistent with current knowledge but our ability to independently quantify such fluxes is also limited.

4.1.2 Potential representation issues

Ideally, a measurement network samples all relevant gradients of the driving factors and magnitudes of the predicted quantities. There are several potential issues with the current sampling by FLUXNET sites. With respect to relevance for net carbon exchange, there are carbon loss pathways that FLUXNET does not capture such as fire emissions, CO₂ evasion from inland waters, and lateral exports due to harvest or erosion that are respired elsewhere (Kirschbaum et al., 2019). The effects of strongly enhanced respiration in the years after large disturbances (Amiro et al., 2010) are challenging to capture due to stochastic and destructive nature of disturbances.

To meet the assumptions of EC method, FLUXNET stations are confined to reasonably flat terrain. Topographic effects on ecosystem fluxes are primarily due to their influence on environmental drivers, i.e., the predictor variables. Thus, the extrapolation to hillslopes should be reasonable if the topographic effects are accounted for in the gridded predictor variables. This might be challenging especially for remote sensing products due to necessary but complicated corrections of illumination conditions. The uncertainties of these topographic factors might become particularly relevant and should be studied for prediction of fluxes at a higher spatial resolution. For the current FLUXCOM products with rather coarse spatial



450 resolution, we expect that topographic effects are reflected in the predictor variables and the remaining subpixel heterogeneity largely cancel out.

Perhaps the most fundamental and frequent critique of the FLUXNET upscaling approach is related to the spatially clumped geographic distribution of EC sites in North America, Europe, Japan, and now Australia with only sparsely distributed towers elsewhere (Schimel et al., 2015). However, what matters eventually for machine learning methods is how well the predictor space, rather than geographic space, is sampled. To assess this, we developed an extrapolation index (EI) that provides indication of the expected additional relative error of a flux prediction due to a large distance to the nearest training data in the predictor space (S2). We applied this method for GPP and FLUXCOM-RS training data as an example, and found that the conditions that are least well represented by FLUXNET are associated to primarily extremely cold and dry regions (Figure 10). Surprisingly, the humid tropics are well represented in the predictor space suggesting that the environmental conditions represented by the predictor set are well sampled by the data from FLUXNET sites. The extremely cold and dry conditions that seem to constitute the biggest extrapolation issues are typically associated with small GPP fluxes and thus also small prediction errors. To account for that, we spatialized the expected GPP error of the RS ensemble (Figure 10, see S2 for details), which largely scales with GPP magnitude but also shows patterns of larger expected errors in semi-arid regions than that expected from flux magnitude alone. The multiplication of the expected GPP error with the extrapolation index provides the extrapolation severity index (ESI) that allows for evaluating where poor FLUXNET sampling likely increases the absolute prediction error strongly. According to these results, sub-tropical semi-arid regions, in particular India, appear as most affected, suggesting that GPP upscaling from FLUXNET would benefit most strongly from improved data availability for towers representing these conditions. Despite these limitations of data, we found excellent consistency of FLUXCOM GPP seasonal cycles with SIF over these regions, which was in fact much better than the consistency between TRENDY models and SIF. This suggests that while more towers in semi-arid regions will help reduce uncertainty in future upscaling efforts, FLUXCOM can already provide useful information for constraining the models in these regions. It also shows that the bias in geographic representation of FLUXNET sites is not as critical as anticipated due to the flexibility and adaptiveness of machine learning methods. The sampled environmental conditions (predictor space) should cover the conditions of the global application domain rather than being representative of it. The larger issue of the FLUXNET representation bias is associated with drawing conclusions from the site-level cross-validation because the evaluation metrics are easily biased towards certain regions and ecosystems.

The methodology used here to assess the extrapolation problem quantitatively has several limitations. For example, potential differences in EC data quality were not accounted for. Perhaps, the largest but unavoidable limitation is the reliance on the predictor set and the assumption that it captures all relevant gradients. In a sense, the methodology can only uncover “known unknowns”. If an important predictor is missing, the method would, of course, not see any extrapolation penalty with respect to the missing factor. Somewhat ironically, we may need more towers in the first place to identify further relevant predictors



485 in an objective way to, say, better capture the diversity in the tropics (Fu et al., 2018) or in agricultural systems (Guanter et al., 2014) where we anticipate that the current sampling is limiting the FLUXCOM approach.

4.2 Driving factors and predictors

Assuming infinite sample size, perfect quality and coverage, the success of machine learning methods depends entirely on the completeness of the predictor set for the target variable, given an adequate training. The predictor set for FLUXNET upscaling is practically constrained by 1) the availability of consistent observations at site level across all sites, and for most
490 of their temporal coverage at a spatial resolution sufficiently close to the flux tower footprint; and 2) the availability of corresponding global grids at an adequate spatial and temporal resolution and temporal coverage. This explains the predictor space of remotely sensed land products from MODIS along with tower-measured meteorology chosen in FLUXCOM. While the general success of the FLUXCOM approach suggests that the predictor sets cover explicitly or implicitly a lot of the necessary information for predicting the variability of carbon fluxes, it is also obvious that some factors are not or, at least,
495 not well accounted for.

4.2.1 Site-history

It has been argued previously (Besnard et al., 2018; Jung et al., 2011; Tramontana et al., 2016) that the current limitations of unrealistic mean NEE patterns from FLUXNET upscaling is also due to missing predictor variables that describe site history effects such as forest age or time since disturbance. These factors have been shown to influence IAV (Musavi et al., 2017; Tamrakar et al., 2018) and to drive mean NEE patterns in synthesis studies (e.g. Amiro et al., 2010). Including forest age in a
500 simple empirical model helped predicting between site variations of mean NEE across FLUXNET sites (Besnard et al., 2018). Counterintuitively, including forest age in training a machine learning method on monthly NEE did not improve the predictability of mean site NEE (Besnard et al., 2019), albeit possibly due to data or methodological limitations. We find the largest discrepancies of mean FLUXCOM NEE with atmospheric inversions in the tropics, where site history plays a
505 substantial role in NEE magnitude (Pugh et al., 2019), but the concept of forest age is hardly applicable due to the generally uneven aged nature of stands, and reliable estimates of gridded age, e.g., from forest inventories are not available. Efforts to incorporate the information from long-term LANDSAT time series to capture site history effects did not reveal an improvement in the predictions of mean NEE, but it remains unclear if this was due to limited information content in these time series or due to methodological issues (Besnard et al., 2019). Thus, this issue remains a significant scientific challenge.
510 Potentially, the availability and application of high-resolution biomass and vegetation optical depth estimates from radar remote sensing along with a carefully collected ancillary data on biomass, basal area, tree diameter and tree age distributions at ICOS and NEON sites may help in the future.



4.2.2 Management

We are presumably lacking important information on anthropogenic management effects, in particular for crops (Guanter et al., 2014) but also for forests. This is primarily due to a lack of information on, e.g., crop type, fertilizer application, irrigation, harvest or thinning at FLUXNET sites, but also due to the still-limited number of crop sites to provide sufficient information on relevant predictors therein. Accounting for the management effects in the FLUXCOM approach either by explicit management information or implicitly by adequate remote sensing data may also help improve the predictions of IAV of local-scale carbon fluxes, in particular with cross-validation since most FLUXNET sites are subject to some degree of management.

4.2.3 CO₂ fertilisation

FLUXCOM lacks any explicit treatment of the effects of CO₂ fertilization causing carbon flux trends to be unrealistic (Fig.S9). This is a challenging problem due to a comparatively small size of [CO₂] effect. This, in turn, makes it particularly vulnerable to distortions through measurement uncertainties, and, on an annual scale, largely indistinguishable from any other factor that varies with time. Potentially, in the future, the availability of longer time series along with high-quality near surface atmospheric CO₂ data at high spatial and temporal resolution at the tower scale could allow for extracting a CO₂ fertilization effect by exploiting diurnal, seasonal, and spatial CO₂ gradients in addition to the long-term trend.

4.2.4 Water stress

Site-level cross-validation analysis (Bodesheim et al., 2018; Tramontana et al., 2016) indicated that soil moisture effects on carbon fluxes are not always well captured. In RS+METEO, moisture effects are explicitly addressed by a simple meteorology driven water availability index. The RS setup relies entirely on indirect information encoded in remotely sensed surface properties such as vegetation indices and land surface temperatures. The comparison of FLUXCOM GPP seasonal cycles with SIF yielded excellent agreement, also in water limited systems, and studies on drought effects using the GPP RS product (Flach et al., 2018; Orth et al., in review; Walther et al., 2019) found plausible patterns that were consistent with independent data on large scales. Nevertheless, we should strive further to improve water stress effects in the upscaling approach given its significance. Better or explicit predictor variables on soil moisture may help. Unfortunately, current soil moisture products from remote sensing are only representative of the top few centimeters and are at comparatively coarse spatial resolution limiting their applicability in reflecting spatial heterogeneities of soil moisture. Perhaps, the larger issue is diverse ecosystem specific responses to soil moisture variations due to different ecosystem compositions, rooting patterns, plant hydraulics, stomata and other physiological traits. Thus, exploring remotely sensed products that reflect additional or complementary information on water stress effects, such as diurnal cycles of land surface temperature from geostationary satellites, is a potential way forward.



4.2.4 Product properties

The success of incorporating novel informative data of site properties in the FLUXCOM approach is always contingent on the quality of the corresponding global gridded products. Systematic differences between a predictor variable used for training at the site-level and global forcing data, as well as any potential artefacts due to retrieval issues or merging different data records spatially or temporally propagate to global flux products. Future improvements of the FLUXCOM approach will thus require progress in other research fields with emphasis on the processing, correction, and harmonization of Earth observation products. Especially for remotely sensed data, strategies to bridge scales of satellite pixels, overpass times, and repeat cycles to continuous measurements of flux footprints are needed. In addition, making use of novel data in the FLUXCOM framework requires the concurrent development of new methodological strategies to cope with the small temporal overlap of the FLUXNET data history. More generally, the quality and quantity of Earth observation data has been increasing rapidly, bringing challenges and opportunities for upscaling.

4.3 Machine learning

4.3.1 Exploiting temporal data structures

The machine learning methods employed in FLUXCOM are classic ones, while novel approaches could bring further improvements. One conceptual limitation of all machine learning methods used in FLUXCOM is that they assume independent and identically distributed (i.i.d.) variables, and thus do not respect or exploit temporal structures in the training data. This problem can be remedied by using other machine learning methods based on convolutions. For example, recurrent neural networks (RNNs) were designed for time-series and can account for dynamics such as ecosystem lag and memory effects on carbon flux variability. Conceptually, lag and memory effects emerge due to the effect of unobserved ecosystem state variables. RNNs can potentially counteract the lack of a relevant state variable in the predictor set if the state variable's instantaneous effect is encoded in the temporal history of other predictor variables (e.g., current soil moisture as a function of previous weather). While exploiting the temporal information of predictors using an RNN improved predictions of monthly carbon fluxes in terms of the seasonal cycle and thereby also across-site variability, predictions of interannual variability were not improved as compared to exploiting only time-instantaneous effects based on site-level cross-validation (Besnard et al., 2019). Further exploration of the machine learning methods that exploit the temporal structure of predictors has a potential to improve FLUXCOM upscaling.

4.3.2 Promising strategies

Deep learning techniques, in general, and convolutional neural networks (CNNs), in particular, have proven to be very powerful especially for image processing and recognition tasks (LeCun et al., 2015). Their conceptual strength lies in the automated extraction of features, in particular those related to spatial structures that render the design and implementation of hand-crafted predictor variables unnecessary. Whether simply employing CNNs for upscaling brings similar improvements



575 over traditional machine learning techniques as in other domains is questionable. This is because the number and spatial
distribution of FLUXNET towers seems insufficient to exploit the power of CNNs to extract relevant features of spatial
structure. However, combining CNNs with transfer learning approaches seems very promising from a conceptual
perspective. The principle of transfer learning is to learn relevant features from a more densely observed proxy variable of
the actual target and use the feature representation for learning the target (Pan and Yang, 2010). The learning of the proxy
variable can be done either prior to or simultaneously with the actual target such that information from much larger sample
580 of the proxy can be transferred to the sparsely observed target variable. This approach could be applicable to the upscaling of
FLUXNET GPP by using remotely sensed SIF as a proxy and thereby alleviate issues related to small sample size (e.g.,
extrapolation) but also aid the extraction of small but relevant signals (e.g., IAV). Spatial structures in high-resolution SIF
data may further encode effects of management or topographically controlled soil moisture variations that could be exploited
with CNNs and improve predictions.

585

Hybrid approaches, i.e. the integration of machine learning method with process understanding and physical constraints, are
another promising avenue. This allows for different strategies and levels of complexity are possible (Reichstein et al., 2019),
and could also greatly help in regularizing machine learning predictions to be sensible under extrapolation conditions. In the
context of FLUXCOM, for, say, constraining the anticipated weak signal of CO₂ fertilization in observations within
590 theoretically derived bounds, would allow this relevant yet observationally poorly constrained dynamic to be incorporated. If
the hybrid approach features the conceptualization of fluxes and pools as in process models, it would also allow for
constraints by multiple complementary data streams simultaneously.

An important aspect to improve in the future is also the quantification of uncertainty in the predictions, including the
595 propagation of observational uncertainties. Gaussian processes can provide probabilistic confidence intervals and allow for
uncertainty propagation, and nowadays have become computationally tractable also for big data problems (Camps-Valls et
al., 2016; Wang et al., 2019). Combining Gaussian Processes with deep neural nets (You et al., 2017) or designing deep
Gaussian process models (Damianou and Lawrence, 2013) are powerful new machine learning tools that may offer solutions
here.

600 **Conclusions**

The FLUXCOM initiative generated a large ensemble of global carbon flux products for two defined setups that differ on the
set of predictor variables and spatial-temporal resolution. The ensemble is comprised of 120 products using up to 9 machine
learning algorithms, two flux-partitioning variants for GPP and TER, and 5 meteorological forcing data sets. The large and
systematically generated ensemble allows for assessing and studying uncertainties of the fluxes as well as the approaches



605 used in FLUXCOM. We assessed FLUXCOM GPP and NEE patterns against remotely sensed sun-induced fluorescence (SIF), atmospheric inversions and process model simulations from the TRENDY initiative.

We found strong consistency of FLUXCOM with SIF and atmospheric inversions with respect to seasonal variations, highlighting FLUXCOM's suitability to evaluate and constrain seasonal cycles for processed-based and top-down
610 approaches. The global GPP from RS+METEO was constrained to 120 ± 7 PgC yr⁻¹ (mean \pm 1 s.d.), while the global GPP from RS (111 ± 3 PgC yr⁻¹) is lower likely due to underestimation in the tropics. FLUXCOM shows a consistently large carbon sink in the tropics that can, at present, not be reconciled with our knowledge derived from atmospheric CO₂ constraints; possibly implying an underestimation of carbon loss and/or missing carbon loss pathways by FLUXNET observations. Patterns of year-to-year variations of the global land carbon sink from FLUXCOM-RS+METEO show good consistency with
615 atmospheric inversions, while magnitudes of interannual variability are underestimated in the data-driven approaches. As FLUXCOM lacks the effect of CO₂ fertilization, trends are not realistic and should only be used for assessing the exclusive effects of climate changes on carbon fluxes.

Moving forward, increasing the size of the FLUXNET network, improving its quality, standardization and coverage will
620 both improve quality and reduce uncertainties in the upscaling approach. This holds especially with respect to signals that are important but relatively small and difficult to extract such as interannual variability or trends. Increasing the number of tropical sites alone would also help constrain global flux magnitudes, and, in particular, would help resolve the large tropical carbon sink shown by FLUXCOM but missing in atmospheric inversions. Based on the number of registered FLUXNET sites alone, an approximate five-fold increase in the number of sites with available data seems feasible in theory; if all
625 respective researchers would contribute their flux data to the global community effort. This indicates that any efforts to improve eddy covariance data, sharing, harmonization and processing are crucial.

Beyond extending the data frame, the current FLUXCOM intercomparison suggests that the next phase of methodological developments should be to move away from predetermined setups and instead towards a set of dedicated experiments that
630 explore novel strategies of data integration with machine learning method (e.g., deep, transfer, and hybrid approaches) and, more importantly, the diversity in the potential predictor space from Earth Observation data. Within FLUXCOM, we find the largest differences between RS and RS+METEO setups which primarily differ in the set of input predictor variables. Thus, the current approach of upscaling FLUXNET measurements seems more information rather than algorithm limited.

635 Overall, the success of FLUXCOM approach depends on the interplay of many different factors. Monitoring our progress will be essential but challenging, and must combine site-level cross-validation, cross-consistency checks with global independent data-streams, novel and dedicated experiments as well as tailored validations of methods with artificial data similar to Observation System Simulation Experiments. Despite the many challenges, integrating eddy covariance ecosystem



scale fluxes, Earth Observation data and machine learning method has already proven valuable in many respects despite
640 being a comparatively new field. An exciting and challenging future lays ahead; that the contribution of experts in different
fields combined with open and real time data sharing could lead to a unique semi-operational carbon monitoring system.
This in turn provides a promising perspective to unify and synergistically exploit data-driven biospheric bottom-up and
atmospheric top-down approaches.

Data availability

645 The FLUXCOM ensemble of carbon fluxes is available upon request to Martin Jung (mjung@bgc-jena.mpg.de) and will be
publically available via the MPI-BGC data portal upon acceptance of this manuscript in Biogeosciences. TRENDY model
output is available on request to Stephen Sitch (S.A.Sitch@exeter.ac.uk).

Author contributions

650 MJ conceived the study, performed the analysis, and drafted the manuscript with intellectual input and extensive edits from
all co-authors.

Competing interests

The authors declare no competing interests.

Acknowledgements

655 The authors acknowledge funding from European Space Agency Climate Change Initiative ESA-CCI RECCAP2 project
(ESRIN/4000123002/18/I-NB), and EU H2020 projects, CHE (GA 776186), VERIFY (GA 776810), E-SHAPE (GA
820852), and BACI (GA 640176). We further want to thank Ana Bastos for input on an earlier version of the manuscript.

References

(C3S), C. C. C. S.: ERA5: Fifth generation of ECMWF atmospheric reanalyses of the global climate. (CDS), C. C. C. S. C.
D. S. (Ed.), 2017.
660 Amiro, B. D., Barr, A. G., Barr, J. G., Black, T. A., Bracho, R., Brown, M., Chen, J., Clark, K. L., Davis, K. J., Desai, A. R.,
Dore, S., Engel, V., Fuentes, J. D., Goldstein, A. H., Goulden, M. L., Kolb, T. E., Lavigne, M. B., Law, B. E., Margolis, H.
A., Martin, T., McCaughey, J. H., Misson, L., Montes-Helu, M., Noormets, A., Randerson, J. T., Starr, G., and Xiao, J.:



- Ecosystem carbon dioxide fluxes after disturbance in forests of North America, *Journal of Geophysical Research: Biogeosciences*, 115, 2010.
- 665 Anav, A., Friedlingstein, P., Beer, C., Ciais, P., Harper, A., Jones, C., Murray-Tortarolo, G., Papale, D., Parazoo, N. C., Peylin, P., Piao, S., Sitch, S., Viovy, N., Wiltshire, A., and Zhao, M.: Spatiotemporal patterns of terrestrial gross primary production: A review, *Reviews of Geophysics*, 53, 785-818, 2015.
- Arnth, A., Sitch, S., Pongratz, J., Stocker, B. D., Ciais, P., Poulter, B., Bayer, A. D., Bondeau, A., Calle, L., Chini, L. P., Gasser, T., Fader, M., Friedlingstein, P., Kato, E., Li, W., Lindeskog, M., Nabel, J. E. M. S., Pugh, T. A. M., Robertson, E.,
- 670 Viovy, N., Yue, C., and Zaehle, S.: Historical carbon dioxide emissions caused by land-use changes are possibly larger than assumed, *Nature Geoscience*, 10, 79, 2017.
- Aubinet, M., Berbigier, P., Bernhofer, C. H., Cescatti, A., Feigenwinter, C., Granier, A., Grunwald, T. H., Havrankova, K., Heinesch, B., Longdoz, B., Marcolla, B., Montagnani, L., and Sedlak, P.: Comparing CO₂ storage and advection conditions at night at different carboeuroflux sites, *Boundary-Layer Meteorology*, 116, 63-94, 2005.
- 675 Aubinet, M., Feigenwinter, C., Heinesch, B., Laffineur, Q., Papale, D., Reichstein, M., Rinne, J., and van Gorsel, E.: Nighttime flux correction. In: *Eddy Covariance: A Practical Guide to Measurement and Data Analysis*, Aubinet, M., Vesala, T., and Papale, D. (Eds.), Springer Atmospheric Sciences, Springer, Dordrecht, 2012.
- Badgley, G., Anderegg, L. D. L., Berry, J. A., and Field, C. B.: Terrestrial gross primary production: Using NIRV to scale from site to globe, *Global Change Biology*, 0, 2019.
- 680 Beer, C., Reichstein, M., Tomelleri, E., Ciais, P., Jung, M., Carvalhais, N., Rödenbeck, C., Arain, M. A., Baldocchi, D., Bonan, G. B., Bondeau, A., Cescatti, A., Lasslop, G., Lindroth, A., Lomas, M., Luysaert, S., Margolis, H., Oleson, K. W., Rouspard, O., Veenendaal, E., Viovy, N., Williams, C., Woodward, F. I., and Papale, D.: Terrestrial gross carbon dioxide uptake: global distribution and covariation with climate, *Science*, 329, 834-838, 2010.
- Besnard, S., Carvalhais, N., Arain, M. A., Black, A., Brede, B., Buchmann, N., Chen, J., Clevers, J. G. P. W., Dutrieux, L.
- 685 P., Gans, F., Herold, M., Jung, M., Kosugi, Y., Knohl, A., Law, B. E., Paul-Limoges, E., Lohila, A., Merbold, L., Rouspard, O., Valentini, R., Wolf, S., Zhang, X., and Reichstein, M.: Memory effects of climate and vegetation affecting net ecosystem CO₂ fluxes in global forests, *PLOS ONE*, 14, e0211510, 2019.
- Besnard, S., Carvalhais, N., Arain, M. A., Black, A., de Bruin, S., Buchmann, N., Cescatti, A., Chen, J., Clevers, J. G. P. W., Desai, A. R., Gough, C. M., Havrankova, K., Herold, M., Hörtnagl, L., Jung, M., Knohl, A., Kruijt, B., Krupkova, L., Law,
- 690 B. E., Lindroth, A., Noormets, A., Rouspard, O., Steinbrecher, R., Varlagin, A., Vincke, C., and Reichstein, M.: Quantifying the effect of forest age in annual net forest carbon balance, *Environmental Research Letters*, 13, 124018, 2018.
- Bodesheim, P., Jung, M., Gans, F., Mahecha, M. D., and Reichstein, M.: Upscaled diurnal cycles of land-atmosphere fluxes: a new global half-hourly data product, *Earth Syst. Sci. Data*, 10, 1327-1365, 2018.
- Byrne, B., Jones, D. B. A., Strong, K., Polavarapu, S. M., Harper, A. B., Baker, D. F., and Maksyutov, S.: On what scales
- 695 can GOSAT flux inversions constrain anomalies in terrestrial ecosystems?, *Atmos. Chem. Phys. Discuss.*, 2019, 1-42, 2019.



- Campioli, M., Malhi, Y., Vicca, S., Luyssaert, S., Papale, D., Peñuelas, J., Reichstein, M., Migliavacca, M., Arain, M. A., and Janssens, I. A.: Evaluating the convergence between eddy-covariance and biometric methods for assessing carbon budgets of forests, *Nature Communications*, 7, 13717, 2016.
- Camps-Valls, G., Verrelst, J., Munoz-Mari, J., Laparra, V., Mateo-Jimenez, F., and Gomez-Dans, J.: A Survey on Gaussian Processes for Earth-Observation Data Analysis: A Comprehensive Investigation, *IEEE Geoscience and Remote Sensing Magazine*, 4, 58-78, 2016.
- 700 Chen, J. M., Mo, G., Pisek, J., Liu, J., Deng, F., Ishizawa, M., and Chan, D.: Effects of foliage clumping on the estimation of global terrestrial gross primary productivity, *Global Biogeochemical Cycles*, 26, 2012.
- Chevallier, F., Fisher, M., Peylin, P., Serrar, S., Bousquet, P., Bréon, F. M., Chédin, A., and Ciais, P.: Inferring CO₂ sources and sinks from satellite observations: Method and application to TOVS data, *Journal of Geophysical Research: Atmospheres*, 110, 2005.
- 705 Chevallier, F., Remaud, M., O'Dell, C. W., Baker, D., Peylin, P., and Cozic, A.: Objective evaluation of surface- and satellite-driven CO₂ atmospheric inversions, *Atmos. Chem. Phys. Discuss.*, 2019, 1-28, 2019.
- Damianou, A. and Lawrence, N.: Deep Gaussian Processes, Scottsdale, AZ, USA2013, 207-215.
- 710 Doelling, D. R., Loeb, N. G., Keyes, D. F., Nordeen, M. L., Morstad, D., Nguyen, C., Wielicki, B. A., Young, D. F., and Sun, M.: Geostationary Enhanced Temporal Interpolation for CERES Flux Products, *J. Atmos. Ocean. Technol.*, 30, 1072-1090, 2013.
- Flach, M., Sippel, S., Gans, F., Bastos, A., Brenning, A., Reichstein, M., and Mahecha, M. D.: Contrasting biosphere responses to hydrometeorological extremes: revisiting the 2010 western Russian heatwave, *Biogeosciences*, 15, 6067-6085, 715 2018.
- Frankenberg, C., Fisher, J. B., Worden, J., Badgley, G., Saatchi, S. S., Lee, J.-E., Toon, G. C., Butz, A., Jung, M., Kuze, A., and Yokota, T.: New global observations of the terrestrial carbon cycle from GOSAT: Patterns of plant fluorescence with gross primary productivity, *Geophysical Research Letters*, 38, L17706, doi:10.1029/2011GL048738, 2011.
- Friedl, M. A., Sulla-Menashe, D., Tan, B., Schneider, A., Ramankutty, N., Sibley, A., and Huang, X.: MODIS Collection 5 global land cover: Algorithm refinements and characterization of new datasets, *Remote Sensing of Environment*, 114, 168-182, 2010.
- 720 Fu, Z., Gerken, T., Bromley, G., Araújo, A., Bonal, D., Burban, B., Ficklin, D., Fuentes, J. D., Goulden, M., Hirano, T., Kosugi, Y., Liddell, M., Nicolini, G., Niu, S., Rouspard, O., Stefani, P., Mi, C., Tofte, Z., Xiao, J., Valentini, R., Wolf, S., and Stoy, P. C.: The surface-atmosphere exchange of carbon dioxide in tropical rainforests: Sensitivity to environmental drivers and flux measurement methodology, *Agricultural and Forest Meteorology*, 263, 292-307, 2018.
- 725 Gaubert, B., Stephens, B. B., Basu, S., Chevallier, F., Deng, F., Kort, E. A., Patra, P. K., Peters, W., Rödenbeck, C., Saeki, T., Schimel, D., Van der Laan-Luijkx, I., Wofsy, S., and Yin, Y.: Global atmospheric CO₂ inverse models converging on neutral tropical land exchange, but disagreeing on fossil fuel and atmospheric growth rate, *Biogeosciences*, 16, 117-134, 2019.



- 730 Guanter, L., Zhang, Y. G., Jung, M., Joiner, J., Voigt, M., Berry, J. A., Frankenberg, C., Huete, A. R., Zarco-Tajada, P., Lee, J.-E., Moran, M. S., Ponce-Campos, G., Beer, C., Camps-Valls, G., Buchmann, N., Gianelle, D., Klumpp, K., Cescatti, A., Baker, J. M., and Griffis, T. J.: Global and time-resolved monitoring of crop photosynthesis with chlorophyll fluorescence, *Proceedings of the National Academy of Sciences of the United States of America*, 111, E1327-E1333, 2014.
- Harris, I. C.: CRU JRA v1.1: A forcings dataset of gridded land surface blend of Climatic Research Unit (CRU) and
735 Japanese reanalysis (JRA) data. Unit, U. o. E. A. C. R. (Ed.), 2019.
- Hayek, M. N., Wehr, R., Longo, M., Hutyra, L. R., Wiedemann, K., Munger, J. W., Bonal, D., Saleska, S. R., Fitzjarrald, D. R., and Wofsy, S. C.: A novel correction for biases in forest eddy covariance carbon balance, *Agricultural and Forest Meteorology*, 250-251, 90-101, 2018.
- Hellevang, H. and Aagaard, P.: Constraints on natural global atmospheric CO₂ fluxes from 1860 to 2010 using a simplified
740 explicit forward model, *Scientific Reports*, 5, 17352, 2015.
- Huffman, G. J., Adler, R. F., Morrissey, M. M., Bolvin, D. T., Curtis, S., Joyce, R., McGavock, B., and Susskind, J.: Global Precipitation at One-Degree Daily Resolution from Multisatellite Observations, *Journal of Hydrometeorology*, 2, 36-50, 2001.
- Humphrey, V., Zscheischler, J., Ciais, P., Gudmundsson, L., Sitch, S., and Seneviratne, S. I.: Sensitivity of atmospheric CO₂
745 growth rate to observed changes in terrestrial water storage, *Nature*, 560, 628-631, 2018.
- Hutyra, L. R., Munger, J. W., Hammond-Pyle, E., Saleska, S. R., Restrepo-Coupe, N., Daube, B. C., de Camargo, P. B., and Wofsy, S. C.: Resolving systematic errors in estimates of net ecosystem exchange of CO₂ and ecosystem respiration in a tropical forest biome, *Agricultural and Forest Meteorology*, 148, 1266-1279, 2008.
- Jiang, C. and Ryu, Y.: Multi-scale evaluation of global gross primary productivity and evapotranspiration products derived
750 from Breathing Earth System Simulator (BESS), *Remote Sensing of Environment*, 186, 528-547, 2016.
- Joiner, J., Yoshida, Y., Zhang, Y., Duveiller, G., Jung, M., Lyapustin, A., Wang, Y., and Tucker, J. C.: Estimation of Terrestrial Global Gross Primary Production (GPP) with Satellite Data-Driven Models and Eddy Covariance Flux Data, *Remote Sensing*, 10, 2018.
- Jung, M., Koirala, S., Weber, U., Ichii, K., Gans, F., Camps-Valls, G., Papale, D., Schwalm, C., Tramontana, G., and
755 Reichstein, M.: The FLUXCOM ensemble of global land-atmosphere energy fluxes, *Scientific Data*, in press, 2019.
- Jung, M., Reichstein, M., and Bondeau, A.: Towards global empirical upscaling of FLUXNET eddy covariance observations: validation of a model tree ensemble approach using a biosphere model, *Biogeosciences*, 6, 2001-2013, 2009.
- Jung, M., Reichstein, M., Margolis, H. A., Cescatti, A., Richardson, A. D., Arain, M. A., Arneeth, A., Bernhofer, C., Bonal, D., Chen, J., Gianelle, D., Gobron, N., Kiely, G., Kutsch, W., Lasslop, G., Law, B. E., Lindroth, A., Merbold, L.,
760 Montagnani, L., Moors, E. J., Papale, D., Sottocornola, M., Vaccari, F., and Williams, C.: Global patterns of land-atmosphere fluxes of carbon dioxide, latent heat, and sensible heat derived from eddy covariance, satellite, and meteorological observations, *Journal of Geophysical Research - Biogeosciences*, 116, G00J07, doi:10.1029/2010JG001566, 2011.



- Jung, M., Reichstein, M., Schwalm, C. R., Huntingford, C., Sitch, S., Ahlström, A., Arneth, A., Camps-Valls, G., Ciais, P.,
765 Friedlingstein, P., Gans, F., Ichii, K., Jain, A. K., Kato, E., Papale, D., Poulter, B., Raduly, B., Rödenbeck, C., Tramontana,
G., Viovy, N., Wang, Y.-P., Weber, U., Zaehle, S., and Zeng, N.: Compensatory water effects link yearly global land CO₂
sink changes to temperature, *Nature*, 541, 516-520, 2017.
- Keenan, T. F., Migliavacca, M., Papale, D., Baldocchi, D., Reichstein, M., Torn, M., and Wutzler, T.: Widespread inhibition
of daytime ecosystem respiration, *Nature Ecology & Evolution*, 3, 407-415, 2019.
- 770 Kim, H.: Global Soil Wetness Project Phase 3 Atmospheric Boundary Conditions (Experiment 1) [Data set]. (DIAS), D. I. a.
A. S. (Ed.), 2017.
- Kirschbaum, M. U. F., Zeng, G., Ximenes, F., Giltrap, D. L., and Zeldis, J. R.: Towards a more complete quantification of
the global carbon cycle, *Biogeosciences*, 16, 831-846, 2019.
- Koffi, E. N., Rayner, P. J., Scholze, M., and Beer, C.: Atmospheric constraints on gross primary productivity and net
775 ecosystem productivity: Results from a carbon-cycle data assimilation system, *Global Biogeochemical Cycles*, 26, 2012.
- Köhler, P., Guanter, L., and Joiner, J.: A linear method for the retrieval of sun-induced chlorophyll fluorescence from
GOME-2 and SCIAMACHY data, *Atmos. Meas. Tech.*, 8, 2589-2608, 2015.
- Lasslop, G., Reichstein, M., Papale, D., Richardson, A. D., Arneth, A., Barr, A., Stoy, P., and Wohlfahrt, G.: Separation of
780 net ecosystem exchange into assimilation and respiration using a light response curve approach: critical issues and global
evaluation, *Global Change Biology*, 16, 187-208, 2010.
- Le Quéré, C., Andrew, R. M., Friedlingstein, P., Sitch, S., Hauck, J., Pongratz, J., Pickers, P. A., Korsbakken, J. I., Peters, G.
P., Canadell, J. G., Arneth, A., Arora, V. K., Barbero, L., Bastos, A., Bopp, L., Chevallier, F., Chini, L. P., Ciais, P., Doney,
S. C., Gkritzalis, T., Goll, D. S., Harris, I., Haverd, V., Hoffman, F. M., Hoppema, M., Houghton, R. A., Hurtt, G., Ilyina, T.,
Jain, A. K., Johannessen, T., Jones, C. D., Kato, E., Keeling, R. F., Goldewijk, K. K., Landschützer, P., Lefèvre, N., Lienert,
785 S., Liu, Z., Lombardozi, D., Metzl, N., Munro, D. R., Nabel, J. E. M. S., Nakaoka, S. I., Neill, C., Olsen, A., Ono, T., Patra,
P., Peregon, A., Peters, W., Peylin, P., Pfeil, B., Pierrot, D., Poulter, B., Rehder, G., Resplandy, L., Robertson, E., Rocher,
M., Rödenbeck, C., Schuster, U., Schwinger, J., Séférian, R., Skjelvan, I., Steinhoff, T., Sutton, A., Tans, P. P., Tian, H.,
Tilbrook, B., Tubiello, F. N., van der Laan-Luijkx, I. T., van der Werf, G. R., Viovy, N., Walker, A. P., Wiltshire, A. J.,
Wright, R., Zaehle, S., and Zheng, B.: Global Carbon Budget 2018, *Earth Syst. Sci. Data*, 10, 2141-2194, 2018.
- 790 LeCun, Y., Bengio, Y., and Hinton, G.: Deep learning, *Nature*, 521, 436, 2015.
- Leuning, R., van Gorsel, E., Massman, W. J., and Isaac, P. R.: Reflections on the surface energy imbalance problem,
Agricultural and Forest Meteorology, 156, 65-74, 2012.
- Liang, M.-C., Mahata, S., Laskar, A. H., Thiemens, M. H., and Newman, S.: Oxygen isotope anomaly in tropospheric CO₂
and implications for CO₂ residence time in the atmosphere and gross primary productivity, *Scientific Reports*, 7, 13180,
795 2017.



- MacBean, N., Maignan, F., Bacour, C., Lewis, P., Peylin, P., Guanter, L., Köhler, P., Gómez-Dans, J., and Disney, M.: Strong constraint on modelled global carbon uptake using solar-induced chlorophyll fluorescence data, *Scientific Reports*, 8, 1973, 2018.
- Marcolla, B., Rödenbeck, C., and Cescatti, A.: Patterns and controls of inter-annual variability in the terrestrial carbon
800 budget, *Biogeosciences*, 14, 3815-3829, 2017.
- McHugh, I. D., Beringer, J., Cunningham, S. C., Baker, P. J., Cavagnaro, T. R., Mac Nally, R., and Thompson, R. M.: Interactions between nocturnal turbulent flux, storage and advection at an “ideal” eucalypt woodland site, *Biogeosciences*, 14, 3027-3050, 2017.
- Migliavacca, M., Perez-Priego, O., Rossini, M., El-Madany, T. S., Moreno, G., van der Tol, C., Rascher, U., Berninger, A.,
805 Bessenbacher, V., Burkart, A., Carrara, A., Fava, F., Guan, J.-H., Hammer, T. W., Henkel, K., Juarez-Alcalde, E., Julitta, T., Kolle, O., Martín, M. P., Musavi, T., Pacheco-Labrador, J., Pérez-Burgueño, A., Wutzler, T., Zaehle, S., and Reichstein, M.: Plant functional traits and canopy structure control the relationship between photosynthetic CO₂ uptake and far-red sun-induced fluorescence in a Mediterranean grassland under different nutrient availability, *New Phytologist*, 214, 1078-1091, 2017.
- 810 Morales, P., Sykes, M. T., Prentice, I. C., Smith, P., Smith, B., Bugmann, H., Zierl, B., Friedlingstein, P., Viovy, N., Sabaté, S., Sánchez, A., Pla, E., Gracia, C. A., Sitch, S., Arneth, A., and Ogee, J.: Comparing and evaluating process-based ecosystem model predictions of carbon and water fluxes in major European forest biomes, *Global Change Biology*, 11, 2211-2233, 2005.
- Musavi, T., Migliavacca, M., Reichstein, M., Kattge, J., Wirth, C., Black, T. A., Janssens, I., Knohl, A., Loustau, D.,
815 Rouspard, O., Varlagin, A., Rambal, S., Cescatti, A., Gianelle, D., Kondo, H., Tamrakar, R., and Mahecha, M. D.: Stand age and species richness dampen interannual variation of ecosystem-level photosynthetic capacity, *Nature Ecology & Evolution*, 1, 0048, 2017.
- Norton, A. J., Rayner, P. J., Koffi, E. N., Scholze, M., Silver, J. D., and Wang, Y. P.: Estimating global gross primary productivity using chlorophyll fluorescence and a data assimilation system with the BETHY-SCOPE model, *Biogeosciences*
820 Discuss., 2019, 1-45, 2019.
- Orth, R., Destouni, G., Jung, M., and Reichstein, M.: Large-scale biospheric drought responses intensifies linearly with drought duration, *Geophysical Research Letters*, in review. in review.
- Pan, S. J. and Yang, Q.: A Survey on Transfer Learning, *IEEE Transactions on Knowledge and Data Engineering*, 22, 1345-1359, 2010.
- 825 Pan, Y., Birdsey, R. A., Fang, J., Houghton, R., Kauppi, P. E., Kurz, W. A., Phillips, O. L., Shvidenko, A., Lewis, S. L., Canadell, J. G., Ciais, P., Jackson, R. B., Pacala, S. W., McGuire, A. D., Piao, S., Rautiainen, A., Sitch, S., and Hayes, D.: A Large and Persistent Carbon Sink in the World’s Forests, *Science*, 333, 988, 2011.
- Papale, D., Black, T. A., Carvalhais, N., Cescatti, A., Chen, J., Jung, M., Kiely, G., Lasslop, G., Mahecha, M. D., Margolis, H., Merbold, L., Montagnani, L., Moors, E., Olesen, J. E., Reichstein, M., Tramontana, G., van Gorsel, E., Wohlfahrt, G.,



- 830 and Ráduly, B.: Effect of spatial sampling from European flux towers for estimating carbon and water fluxes with artificial neural networks, *Journal of Geophysical Research: Biogeosciences*, 120, 1941-1957, 2015.
- Papale, D., Reichstein, M., Aubinet, M., Canfora, E., Bernhofer, C., Kutsch, W., Longdoz, B., Rambal, S., Valentini, R., Vesala, T., and Yakir, D.: Towards a standardized processing of Net Ecosystem Exchange measured with eddy covariance technique: algorithms and uncertainty estimation, *Biogeosciences*, 3, 571-583, 2006.
- 835 Peters, W., Krol, M. C., Van Der Werf, G. R., Houweling, S., Jones, C. D., Hughes, J., Schaefer, K., Matarie, K. A., Jacobson, A. R., Miller, J. B., Cho, C. H., Ramonet, M., Schmidt, M., Ciattaglia, L., Apadula, F., Heltai, D., Meinhardt, F., Di Sarra, A. G., Piacentino, S., Sferlazzo, D., Aalto, T., Hatakka, J., StrÖM, J., Haszpra, L., Meijer, H. A. J., Van Der Laan, S., Neubert, R. E. M., Jordan, A., RodÓ, X., MorguÍ, J. A., Vermeulen, A. T., Popa, E., Rozanski, K., Zimnoch, M., Manning, A. C., Leuenberger, M., Uglietti, C., Dolman, A. J., Ciais, P., Heimann, M., and Tans, P. P.: Seven years of recent
840 European net terrestrial carbon dioxide exchange constrained by atmospheric observations, *Global Change Biology*, 16, 1317-1337, 2010.
- Peylin, P., Law, R. M., Gurney, K. R., Chevallier, F., Jacobson, A. R., Maki, T., Niwa, Y., Patra, P. K., Peters, W., Rayner, P. J., Roedenbeck, C., van der Laan-Luijkx, I. T., and Zhang, X.: Global atmospheric carbon budget: results from an ensemble of atmospheric CO₂ inversions, *Biogeosciences*, 10, 6699-6720, 2013.
- 845 Porcar-Castell, A., Tyystjärvi, E., Atherton, J., van der Tol, C., Flexas, J., Pfündel, E. E., Moreno, J., Frankenberg, C., and Berry, J. A.: Linking chlorophyll a fluorescence to photosynthesis for remote sensing applications: mechanisms and challenges, *Journal of Experimental Botany*, 65, 4065-4095, 2014.
- Pugh, T. A. M., Arneeth, A., Kautz, M., Poulter, B., and Smith, B.: Important role of forest disturbances in the global biomass turnover and carbon sinks, *Nature Geoscience*, 12, 730-735, 2019.
- 850 Reichstein, M., Camps-Valls, G., Stevens, B., Jung, M., Denzler, J., Carvalhais, N., and Prabhat: Deep learning and process understanding for data-driven Earth system science, *Nature*, 566, 195-204, 2019.
- Reichstein, M., Falge, E., Baldocchi, D., Papale, D., Valentini, R., Aubinet, M., Berbigier, P., Bernhofer, C., Buchmann, N., Gilmanov, T., Granier, A., Grünwald, T., Havránková, K., Janous, D., Knohl, A., Laurela, T., Lohila, A., Loustau, D., Matteucci, G., Meyers, T., Miglietta, F., Ourcival, J.-M., Rambal, S., Rotenberg, E., Sanz, M., Seufert, G., Vaccari, F.,
855 Vesala, T., and Yakir, D.: On the separation of net ecosystem exchange into assimilation and ecosystem respiration: review and improved algorithm, *Global Change Biology*, 11, 1424-1439, 2005.
- Rödenbeck, C., Zachle, S., Keeling, R., and Heimann, M.: How does the terrestrial carbon exchange respond to inter-annual climatic variations? A quantification based on atmospheric CO₂ data, *Biogeosciences*, 15, 2481-2498, 2018.
- Saleska, S. R., Miller, S. D., Matross, D. M., Goulden, M. L., Wofsy, S. C., da Rocha, H. R., de Camargo, P. B., Crill, P.,
860 Daube, B. C., de Freitas, H. C., Hutyrá, L., Keller, M., Kirchner, V., Menton, M., Munger, J. W., Pyle, E. H., Rice, A. H., and Silva, H.: Carbon in Amazon Forests: Unexpected Seasonal Fluxes and Disturbance-Induced Losses, *Science*, 302, 1554, 2003.



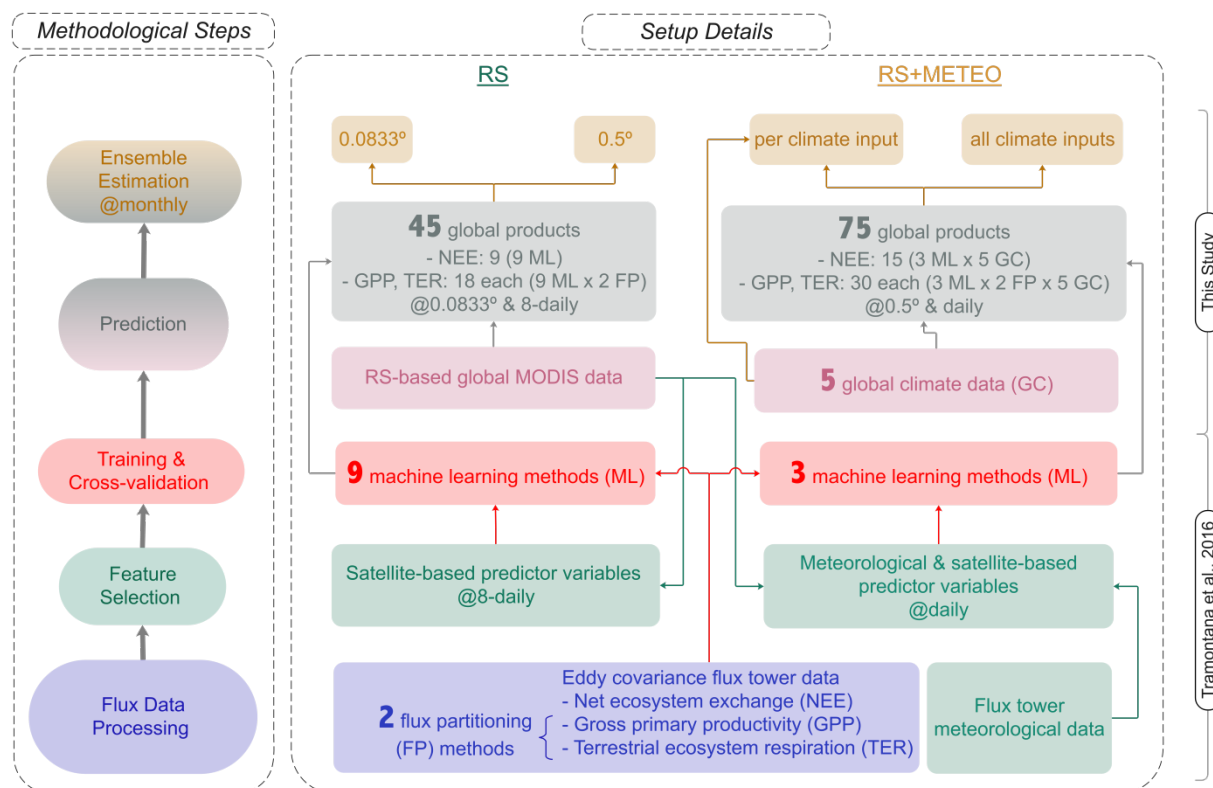
- Schimel, D., Pavlick, R., Fisher, J. B., Asner, G. P., Saatchi, S., Townsend, P., Miller, C., Frankenberg, C., Hibbard, K., and Cox, P.: Observing terrestrial ecosystems and the carbon cycle from space, *Global Change Biology*, 21, 1762-1776, 2015.
- 865 Sitch, S., Friedlingstein, P., Gruber, N., Jones, S. D., Murray-Tortarolo, G., Ahlstrom, A., Doney, S. C., Graven, H., Heinze, C., Huntingford, C., Levis, S., Levy, P. E., Lomas, M., Poulter, B., Viovy, N., Zaehle, S., Zeng, N., Arnoeth, A., Bonan, G., Bopp, L., Canadell, J. G., Chevallier, F., Ciais, P., Ellis, R., Gloor, M., Peylin, P., Piao, S. L., Le Quere, C., Smith, B., Zhu, Z., and Myneni, R.: Recent trends and drivers of regional sources and sinks of carbon dioxide, *Biogeosciences*, 12, 653-679, 2015.
- 870 Spielmann, F. M., Wohlfahrt, G., Hammerle, A., Kitz, F., Migliavacca, M., Alberti, G., Ibrom, A., El-Madany, T. S., Gerdel, K., Moreno, G., Kolle, O., Karl, T., Peressotti, A., and Delle Vedove, G.: Gross Primary Productivity of Four European Ecosystems Constrained by Joint CO₂ and COS Flux Measurements, *Geophysical Research Letters*, 46, 5284-5293, 2019.
- Stoy, P. C., Mauder, M., Foken, T., Marcolla, B., Boegh, E., Ibrom, A., Arain, M. A., Arnoeth, A., Aurela, M., Bernhofer, C., Cescatti, A., Dellwik, E., Duce, P., Gianelle, D., van Gorsel, E., Kiely, G., Knohl, A., Margolis, H., McCaughey, H.,
- 875 Merbold, L., Montagnani, L., Papale, D., Reichstein, M., Saunders, M., Serrano-Ortiz, P., Sottocornola, M., Spano, D., Vaccari, F., and Varlagin, A.: A data-driven analysis of energy balance closure across FLUXNET research sites: The role of landscape scale heterogeneity, *Agricultural and Forest Meteorology*, 171-172, 137-152, 2013.
- Sun, Y., Frankenberg, C., Wood, J. D., Schimel, D. S., Jung, M., Guanter, L., Drewry, D. T., Verma, M., Porcar-Castell, A., Griffiths, T. J., Gu, L., Magney, T. S., Köhler, P., Evans, B., and Yuen, K.: OCO-2 advances photosynthesis observation from
- 880 space via solar-induced chlorophyll fluorescence, *Science*, 358, eaam5747, 2017.
- Tamrakar, R., Rayment, M. B., Moyano, F., Mund, M., and Knohl, A.: Implications of structural diversity for seasonal and annual carbon dioxide fluxes in two temperate deciduous forests, *Agricultural and Forest Meteorology*, 263, 465-476, 2018.
- Tramontana, G., Jung, M., Schwalm, C. R., Ichii, K., Camps-Valls, G., Ráduly, B., Reichstein, M., Arain, M. A., Cescatti, A., Kiely, G., Merbold, L., Serrano-Ortiz, P., Sickert, S., Wolf, S., and Papale, D.: Predicting carbon dioxide and energy
- 885 fluxes across global FLUXNET sites with regression algorithms, *Biogeosciences*, 13, 4291-4313, 2016.
- van der Laan-Luijkx, I. T., van der Velde, I. R., van der Veen, E., Tsuruta, A., Stanislawski, K., Babenhauerheide, A., Zhang, H. F., Liu, Y., He, W., Chen, H., Masarie, K. A., Krol, M. C., and Peters, W.: The CarbonTracker Data Assimilation Shell (CTDAS) v1.0: implementation and global carbon balance 2001–2015, *Geosci. Model Dev.*, 10, 2785-2800, 2017.
- van Gorsel, E., Delpierre, N., Leuning, R., Black, A., Munger, J. W., Wofsy, S., Aubinet, M., Feigenwinter, C., Beringer, J.,
- 890 Bonal, D., Chen, B., Chen, J., Clement, R., Davis, K. J., Desai, A. R., Dragoni, D., Etzold, S., Grünwald, T., Gu, L., Heinesch, B., Hutryra, L. R., Jans, W. W. P., Kutsch, W., Law, B. E., Leclerc, M. Y., Mammarella, I., Montagnani, L., Noormets, A., Rebmann, C., and Wharton, S.: Estimating nocturnal ecosystem respiration from the vertical turbulent flux and change in storage of CO₂, *Agricultural and Forest Meteorology*, 149, 1919-1930, 2009.
- van Gorsel, E., Leuning, R., Cleugh, H. A., Keith, H., Kirschbaum, M. U. F., and Suni, T.: Application of an alternative
- 895 method to derive reliable estimates of nighttime respiration from eddy covariance measurements in moderately complex topography, *Agricultural and Forest Meteorology*, 148, 1174-1180, 2008.



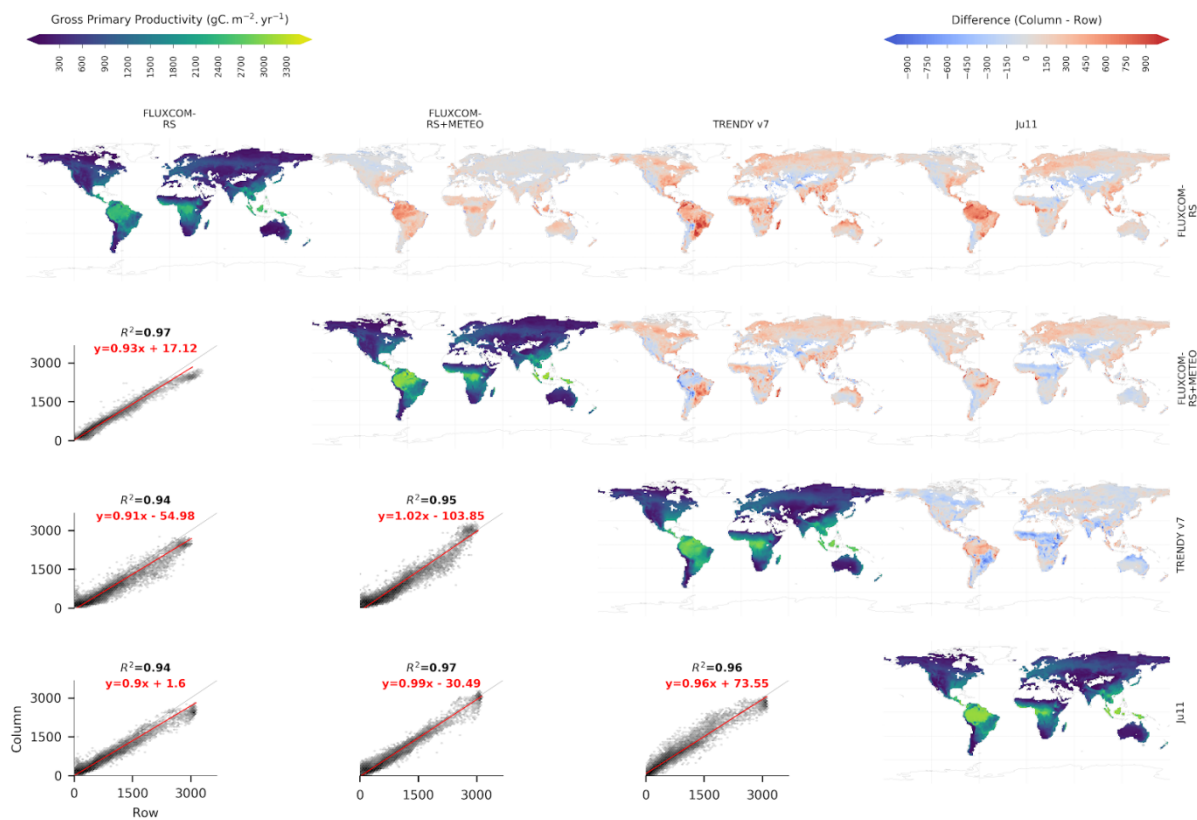
- Walther, S., Duveiller, G., Jung, M., Guanter, L., Cescatti, A., and Camps-Valls, G.: Satellite Observations of the Contrasting Response of Trees and Grasses to Variations in Water Availability, *Geophysical Research Letters*, 46, 1429-1440, 2019.
- 900 Walther, S., Voigt, M., Thum, T., Gonsamo, A., Zhang, Y. G., Kohler, P., Jung, M., Varlagin, A., and Guanter, L.: Satellite chlorophyll fluorescence measurements reveal large-scale decoupling of photosynthesis and greenness dynamics in boreal evergreen forests, *Global Change Biology*, 22, 2979-2996, 2016.
- Wang, K. A., Pleiss, G., Gardner, J. R., Tyree, S., Weinberger, K. Q., and Wilson, A. G.: Exact Gaussian Processes on a Million Data Points, *arXiv*, 2019. 2019.
- 905 Weedon, G. P., Balsamo, G., Bellouin, N., Gomes, S., Best, M. J., and Viterbo, P.: The WFDEI meteorological forcing data set: WATCH Forcing Data methodology applied to ERA-Interim reanalysis data, *Water Resources Research*, 50, 7505-7514, 2014.
- Wehr, R., Munger, J. W., McManus, J. B., Nelson, D. D., Zahniser, M. S., Davidson, E. A., Wofsy, S. C., and Saleska, S. R.: Seasonality of temperate forest photosynthesis and daytime respiration, *Nature*, 534, 680, 2016.
- 910 Welp, L. R., Keeling, R. F., Meijer, H. A. J., Bollenbacher, A. F., Piper, S. C., Yoshimura, K., Francey, R. J., Allison, C. E., and Wahlen, M.: Interannual variability in the oxygen isotopes of atmospheric CO₂ driven by El Niño, *Nature*, 477, 579, 2011.
- You, J., Li, X., Low, M., Lobell, D., and Ermon, S.: Deep Gaussian Process for Crop Yield Prediction Based on Remote Sensing Data, 2017.
- 915 Yu, T., Sun, R., Xiao, Z., Zhang, Q., Liu, G., Cui, T., and Wang, J.: Estimation of Global Vegetation Productivity from Global LAnd Surface Satellite Data, *Remote Sensing*, 10, 2018.
- Yuan, W., Liu, S., Yu, G., Bonnefond, J.-M., Chen, J., Davis, K., Desai, A. R., Goldstein, A. H., Gianelle, D., Rossi, F., Suyker, A. E., and Verma, S. B.: Global estimates of evapotranspiration and gross primary production based on MODIS and global meteorology data, *Remote Sensing of Environment*, 114, 1416-1431, 2010.
- 920 Zhang, Y., Guanter, L., Berry, J. A., van der Tol, C., Yang, X., Tang, J., and Zhang, F.: Model-based analysis of the relationship between sun-induced chlorophyll fluorescence and gross primary production for remote sensing applications, *Remote Sensing of Environment*, 187, 145-155, 2016.
- Zhang, Y., Joiner, J., Gentine, P., and Zhou, S.: Reduced solar-induced chlorophyll fluorescence from GOME-2 during Amazon drought caused by dataset artifacts, *Global Change Biology*, 24, 2229-2230, 2018.
- 925 Zhao, M., Heinsch, F. A., Nemani, R. R., and Running, S. W.: Improvements of the MODIS terrestrial gross and net primary production global data set, *Remote Sensing of Environment*, 95, 164-176, 2005.
- Zscheischler, J., Mahecha, M. D., Avitabile, V., Calle, L., Carvalhais, N., Ciais, P., Gans, F., Gruber, N., Hartmann, J., Herold, M., Ichii, K., Jung, M., Landschützer, P., Laruelle, G. G., Lauerwald, R., Papale, D., Peylin, P., Poulter, B., Ray, D., Regnier, P., Rödenbeck, C., Roman-Cuesta, R. M., Schwalm, C., Tramontana, G., Tyukavina, A., Valentini, R., van der



930 Werf, G., West, T. O., Wolf, J. E., and Reichstein, M.: Reviews and syntheses: An empirical spatiotemporal description of
 the global surface–atmosphere carbon fluxes: opportunities and data limitations, *Biogeosciences*, 14, 3685-3703, 2017.



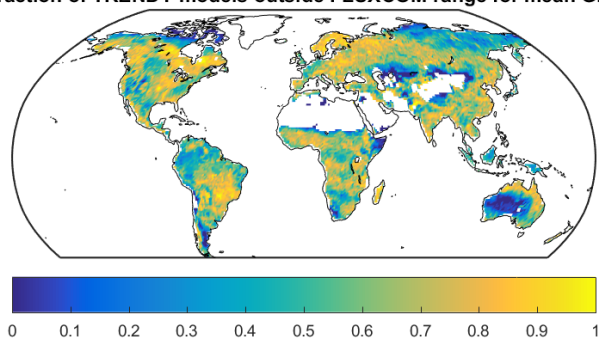
935 **Figure 1: Schematic overview of the methodology and data products from the FLUXCOM initiative. The flow diagram shows the**
methodological steps for the remote sensing -based (RS, left) and the remote sensing and meteorological data -based (RS+METEO,
right) FLUXCOM products. Final monthly ensemble products for NEE, GPP, and TER from RS are available at 0.0833° and at
0.5° spatial resolution. Ensemble products from RS+METEO are available per climate forcing (GC) data set as well as a pooled
ensemble at 0.5° spatial resolution. All ensemble products encompass ensemble members of different machine learning methods
 940 **(ML, 9 for RS, 3 for RS+METEO) and flux partitioning methods (FP, 2 for GPP and TER).**



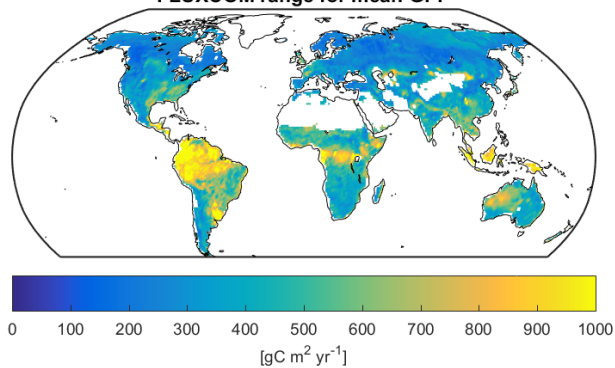
945 **Figure 2:** Comparisons of mean annual GPP at 1° spatial resolution for the period 2008-2010 of FLUXCOM ensemble products with Ju11 and the mean of 16 TRENDY models. **Diagonal:** Maps of mean annual GPP. **Above diagonal:** Maps of GPP differences (product along column – product along row). **Below diagonal:** 1:1 regression where the shading shows point density. The red line and equations show the best fit line from total least square regression.



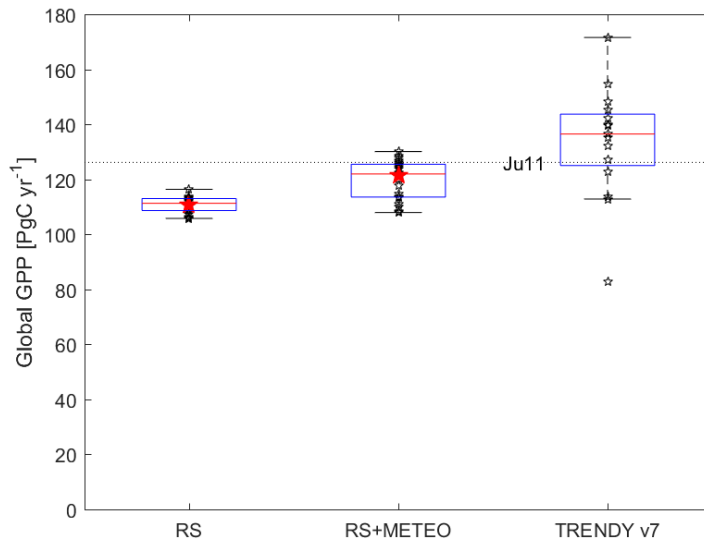
Fraction of TRENDY models outside FLUXCOM range for mean GPP



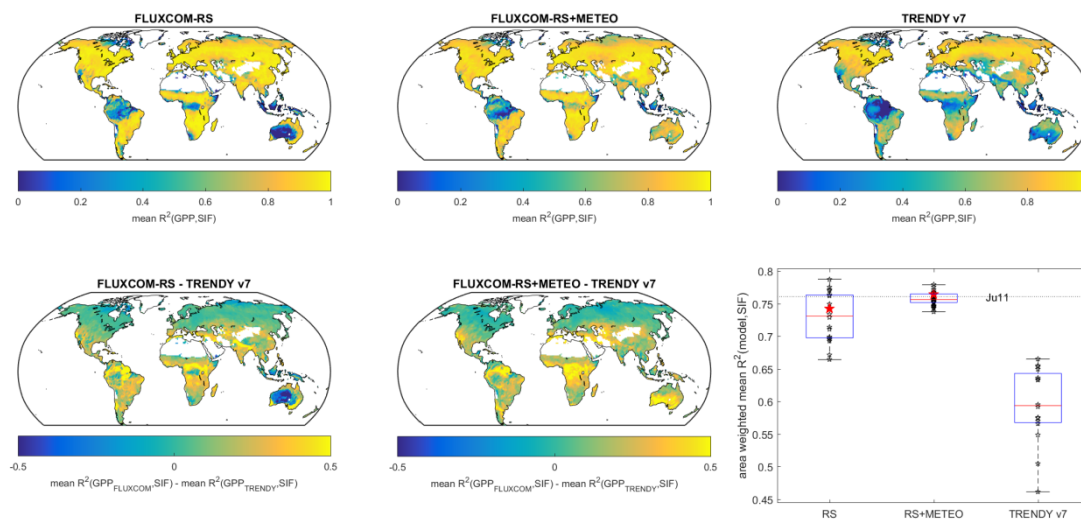
FLUXCOM range for mean GPP



950 **Figure 3: Map of the fraction of TRENDY models (n=16) with mean GPP outside the range of FLUXCOM estimates. The FLUXCOM range is calculated as the maximum minus minimum of all 48 FLUXCOM members from the union of the RS and RS+METEO members. Mean GPP was calculated for the period 2008-2010.**



955 **Figure 4: Global GPP for FLUXCOM and TRENDY ensembles for the period 2008-2010. The box plots show the median (red line), interquartile range (box) and total range (whiskers) of non-outliers (within median \pm 1.5 interquartile range) of individual ensemble members (open black stars). The filled red star presents the value of the ensemble product (not available for TRENDY). The estimate of Ju11 is plotted as horizontal broken line.**



960 **Figure 5: Consistency of seasonal GPP variations from FLUXCOM and TRENDY with SIF from GOME-2. Maps in the top row**
show the mean R^2 between mean seasonal cycles for the period 2008-2010, averaged across all respective ensemble members.
Difference maps in the bottom row emphasize where FLUXCOM shows better (positive value) and worse (negative value)
consistency with SIF than TRENDY and are based on the maps in the top row. The spatially averaged R^2 values for the different
ensembles are summarized in the bottom right panel. The box plots show the distribution of individual ensemble members (open
black stars). The filled red star presents the value of the ensemble product (not available for TRENDY). The estimate of Ju11
965 **is plotted as horizontal broken line.**

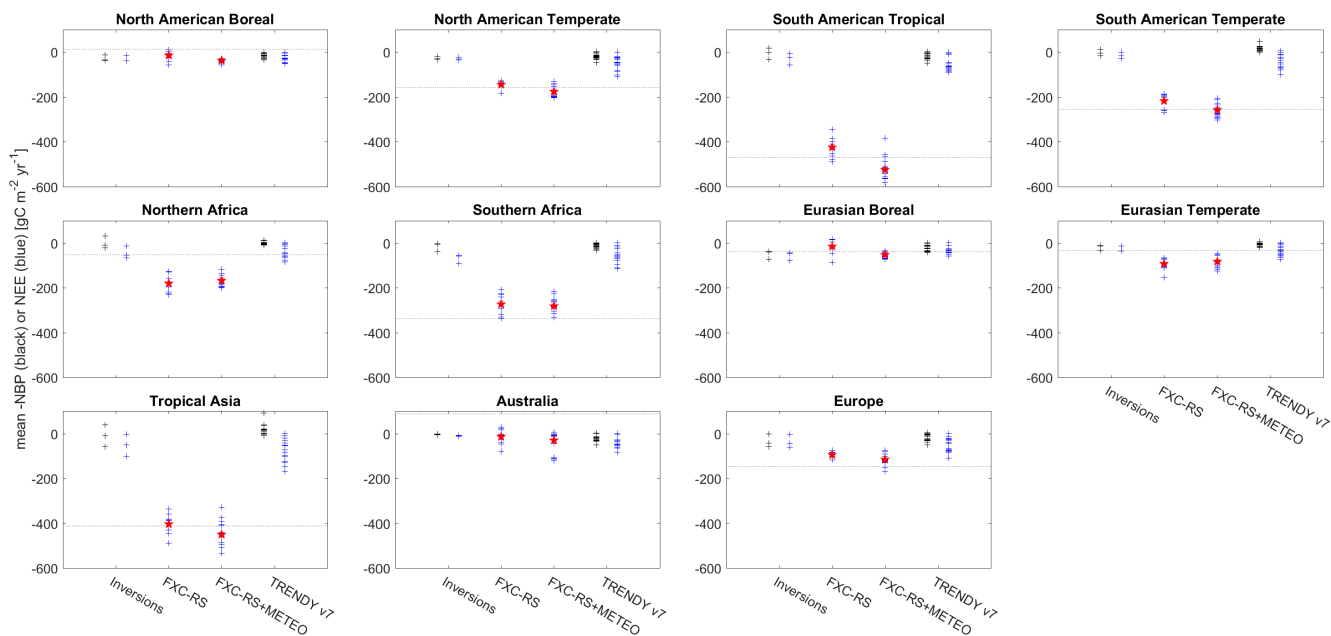
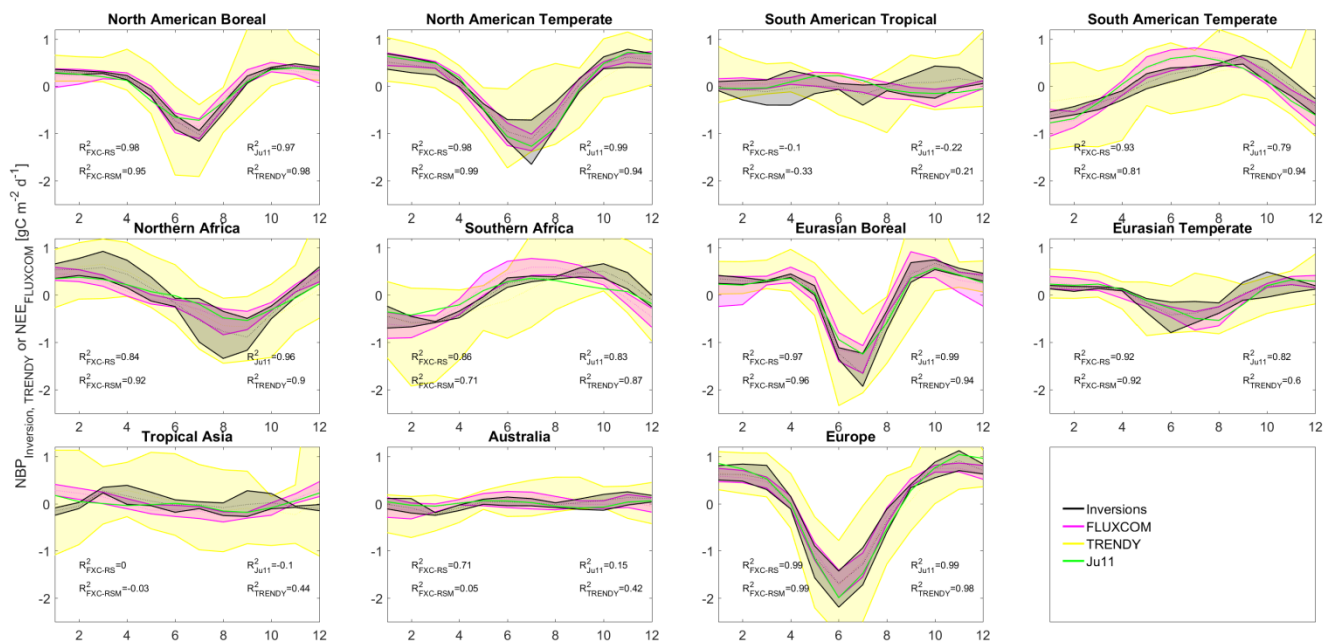


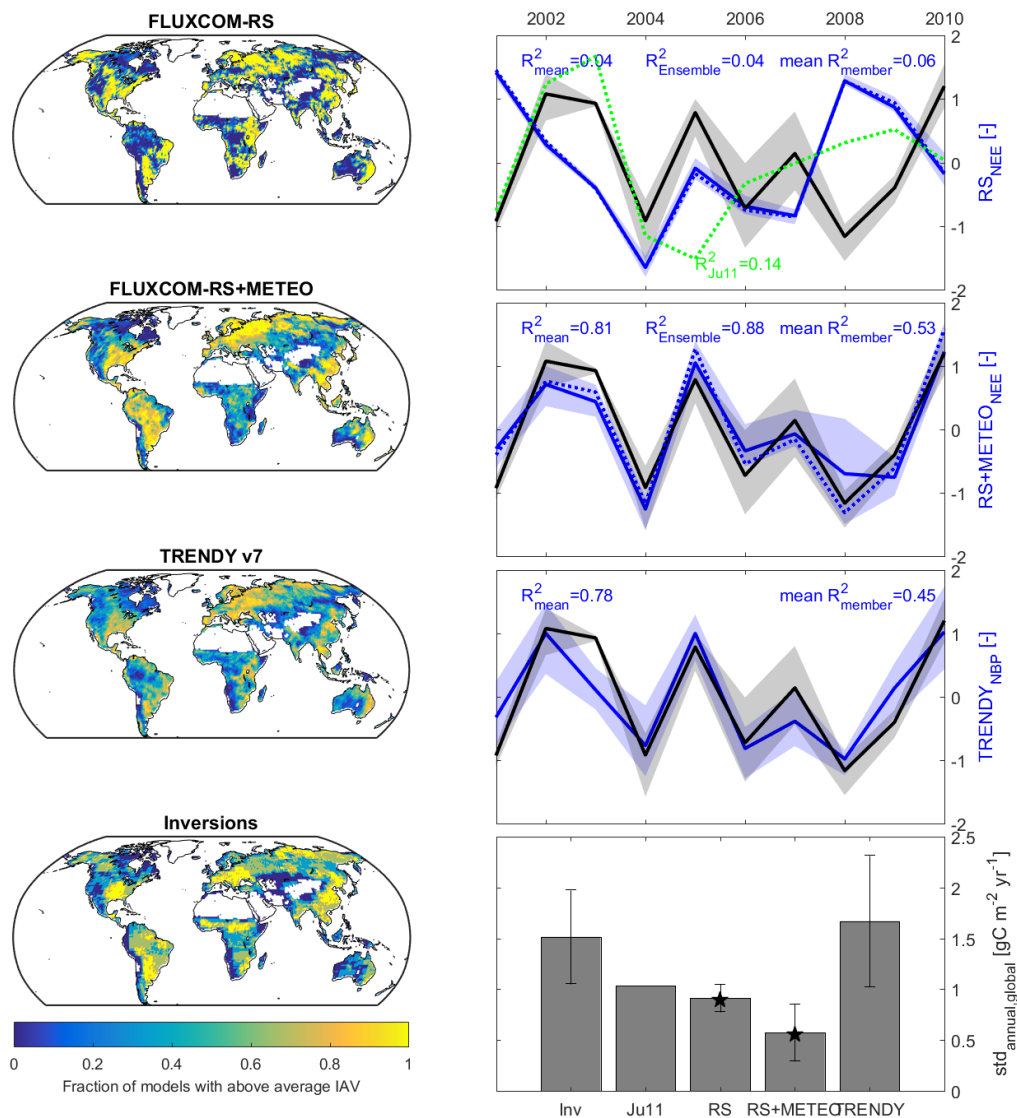
Figure 6: Mean annual net carbon release for the years 2008–2010 over TRANSCOM regions. Crosses refer to individual ensemble members where a black colour refers to negative net biome productivity (NBP, not available for FLUXCOM), and blue colour refers to net ecosystem exchange (NEE). For inversions, NEE was approximated by correcting NBP with fire emissions (see section 2.4.3). The filled red stars refer to estimates by the ensemble product of FLUXCOM setups. The horizontal broken line indicates the estimate of Ju11.

970



975 **Figure 7: Mean seasonal variations of net land carbon release for the period 2008-2010 over TRANSCOM regions. For inversions and TRENDY, -NBP was plotted, and for FLUXCOM, NEE was plotted. Please note that the region specific mean was removed for each data set. Shading indicates the range of estimates (maximum – minimum). The FLUXCOM range is based on the union of RS and RS+METEO ensemble members. R^2 values were calculated with the mean of the inversions. The FLUXCOM RS and RS+METEO refer to the ensemble products (median), while that for TRENDY refer to the model mean.**

980



985 **Figure 8: Interannual variability patterns of FLUXCOM NEE, TRENDY NBP, and NBP from three atmospheric inversions for**
the period 2001-2010. Maps show the fraction of respective ensemble members with above average interannual variability
(standard deviation of annual values multiplied with land area). Time series plots show detrended globally integrated annual NEE
or NBP anomalies normalized by their standard deviation. The black line is the mean of three inversions and the gray shading
indicates their range. The blue solid lines are the means of the considered ensembles; the blue dashed lines are the FLUXCOM
ensemble products. R^2 values refer to the comparison with the mean of inversions (black solid line). The bar chart in the bottom
right panel shows the standard deviation of detrended annual NEE or NBP for different data sets, averaged over the ensemble
members and the error bar indicates the standard deviation of the ensemble members. Black stars for FLUXCOM refer to the
 990 **value for the ensemble products.**

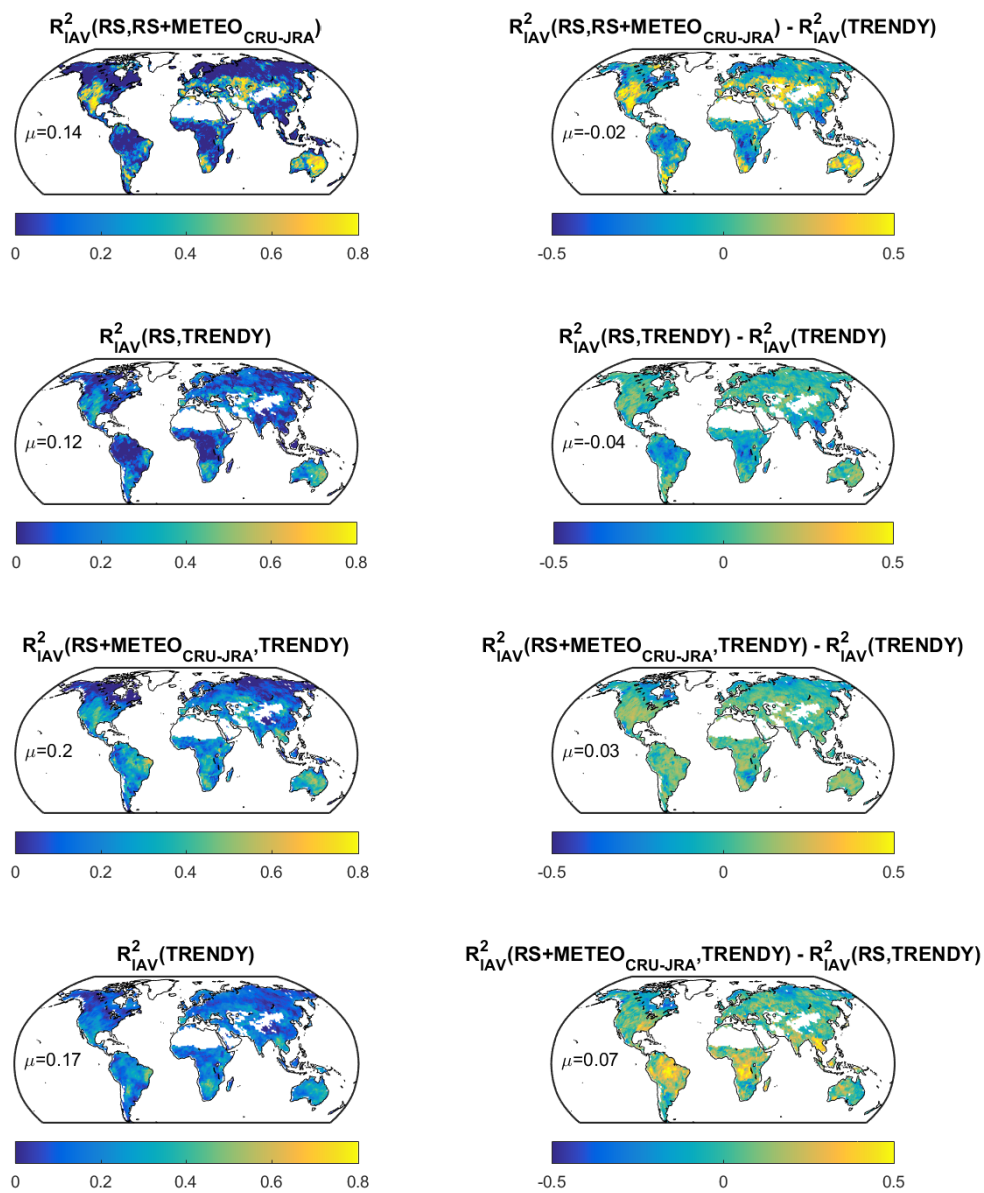
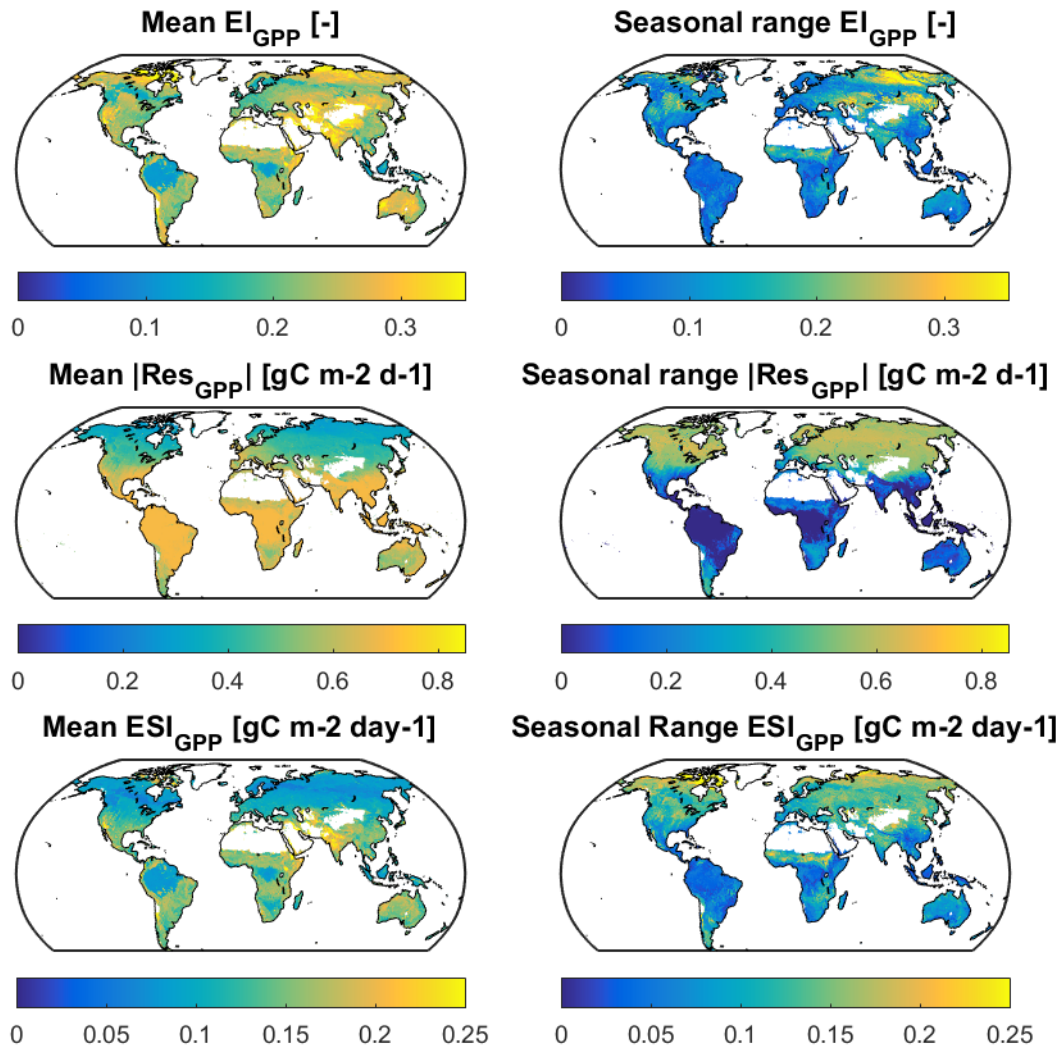


Figure 9: Consistency between interannual variabilities (IAV) of local NEE from FLUXCOM setups and TRENDY for the period 2001-2015.



1000 **Figure 10:** Mean annual (2001-2015) and seasonal range (8-daily time step) of the Extrapolation Index (EI), the expected mean absolute error of machine learning predictions, and the Extrapolation Severity Index (ESI, product of the previous two) (see S2 for details) for GPP from FLUXCOM-RS.



Meteorological forcing data set	Spatial Resolution	Temporal Coverage
CRU-JRA	0.5° x 0.5°	1950-2017
GSWP3	0.5° x 0.5°	1950-2010
WFDEI	0.5° x 0.5°	1979-2013
ERA-5	0.5° x 0.5°	1979-2018
CERES-GPCP	1.0° x 1.0° resampled to 0.5° x 0.5°	2001-2013

Table 1: Global meteorological forcing data sets used in FLUXCOM-RS+METEO.